Jessica Tatianne Ortiz Florenciano

Hierarchical structured ceramic membranes obtained by centrifugal casting using an *in silico* approach

Florianópolis

2021

Jessica Tatianne Ortiz Florenciano

Hierarchical structured ceramic membranes obtained by centrifugal casting using an *in silico* approach

Florianópolis

2021

Ficha de identificação da obra elaborada pelo autor,
através do Programa de Geração Automática da Biblioteca Universitária da UFSC.

Jessica Tatianne Ortiz Florenciano

Hierarchical structured ceramic membranes obtained by centrifugal casting using an *in silico* approach

O presente trabalho em nível de mestrado foi avaliado e aprovado por banca examinadora composta pelos seguintes membros:

Prof. Agenor de Noni Junior, Dr.
Universidade Federal de Santa Catarina (UFSC)

Prof. Maksym Dosta, Dr.
Universidade Técnica de Hamburg (TUHH)

Certificamos que esta é a **versão original e final** do trabalho de conclusão que foi julgado adequado para obtenção do título de mestre em Engenharia Química.

_____
Coordenação do Programa de Pós-Graduação

_____
Prof. Sergio Yesid Gómez González, Dr.
Orientador

Florianópolis, 2021.

This work is dedicated to my dearest grandmother Juanita.

ACKNOWLEDGEMENTS

"What we know is a drop, what we don't know is an ocean."

(Isaac Newton)

RESUMO

O *Centrifugal casting* é uma técnica de moldagem destinada à fabricação de estruturas cerâmicas tubulares, onde o tamanho e a densidade das partículas são utilizados para produzir materiais com gradiente funcional e membranas assimétricas. Contudo, algumas ideias bem estabelecidas sobre os fenômenos de segregação são discutíveis e permanecem inconclusivas. Por exemplo, as partículas menores não necessariamente concentram-se na região interna e as partículas maiores não se acumulam na externa. A partir deste ponto, vários parâmetros de processamento foram estudados através do planejamento robusto de Taguchi, usando simulação baseada no método de elementos discretos para gerar os dados. Pós de alumina e níquel foram empregados como materiais modelo para avaliar o tempo de formação, a espessura, a circularidade, e as mudanças na densidade relativa e na distribuição de tamanho de partícula ao longo da seção transversal do tubo à verde. O diâmetro médio de partícula e a velocidade de rotação são os parâmetros mais influentes no tempo de formação. A fração volumétrica de sólidos na suspensão precursora é decisiva em relação às propriedades estruturais do tubo, e a segregação de partículas é desprezível, exceto para diferenças de tamanho acima de uma ordem de grandeza. A segregação devido à densidade também foi observada, mas as diferenças de tamanho podem facilmente ofuscar seu efeito, conforme confirmado por meio de trabalhos experimentais.

Palavras-chave: Centrifugal casting. Método de elementos discretos. Planejamento robusto. Segregação por tamanho. Material com gradiente funcional.

RESUMO EXPANDIDO

Introdução

Nas ultimas décadas, as membranas cerâmicas ganharam relevância nos processos de separação por membrana devido as suas elevadas estabilidades química, térmica e mecânica. Essas propriedades as tornam adequadas para um grande número de aplicações.

O processamento de membranas cerâmicas geralmente envolve um grande número de etapas. Essas etapas são realizadas sob condições que alteram a estrutura e as propriedades do produto final. Compreender a influência de cada condição de processo sobre o resultado pode levar à obtenção da membrana mais adequada para uma aplicação específica. No geral, as membranas cerâmicas são estruturas hierárquicas assimétricas divididas em camadas. A camada porosa de suporte é comumente fabricada seguindo três etapas: formação da suspensão, conformação do tubo verde e sinterização.

Algumas técnicas de conformação incluem ao *centrifugal casting*. Os tubos verdes moldados por esta técnica podem oferecer uma estrutura mais homogênea com uma superfície interna mais arredondada e lisa em relação à extrusão. Portanto, eles são considerados de qualidade superior para posterior sinterização e, por fim, revestimento com as camadas restantes.

Além disso, o *centrifugal casting* permite a formação de uma estrutura hierárquica uma vez que os tubos verdes podem ter uma gradiente de porosidade, portanto, uma distribuição de tamanho de poro diferente ao longo da seção transversal. Dependendo das condições de fabricação, tanto o suporte quanto as camadas intermediárias podem ser fabricados ao mesmo tempo, reduzindo o custo de processamento da membrana.

Apesar dos esforços prévios, o conhecimento sobre o *centrifugal casting* é insuficiente para prever as influências corretas dadas por um conjunto de condições de processo aos fenômenos de segregação por densidade ou tamanho de partícula em relação à estrutura do tubo verde. Neste trabalho, se investiga a influência dos parâmetros de processamento na avaliação da segregação das partículas por tamanho e densidade, e sua relação com a densidade relativa do tubo, usando uma abordagem de simulação baseada no método de elementos discretos combinada com um planejamento robusto de experimentos.

Objetivos

O objetivo principal deste trabalho é contribuir na área de pesquisa de *centrifugal casting* para o processamento de membranas cerâmicas, identificando parâmetros chave no processo e seu efeito na estrutura do tubo verde. A fim de alcançar este objetivo principal, as seguintes etapas foram definidas:

• Validar uma ferramenta adaptada de simulação baseada no método de elementos discretos para representar sistemas de *centrifugal casting* utilizando informação da literatura.

• Avaliar o efeito de parâmetros selecionados na manufatura de estruturas tubulares utilizando planejamento robusto de experimentos.

• Aferir a segregação das partículas ao longo da seção transversal do tubo à verde devido ao tamanho e a densidade das partículas.

• Realizar experimentos de bancada para verificar os resultados obtidos através das simulações.

Metodologia

O processo de *centrifugal casting* foi realizado *in silico* usando uma estrutura de simulação baseado no método de elementos discretos de código aberto chamado MUSEN. O sistema

inicial consistiu em uma suspensão aquosa de α-alumina, girada horizontalmente em um molde cilíndrico de aço inoxidável 304, com a força da gravidade atuando de forma vertical e descendente sobre o sistema. Foram incorporados o modelo de contato de Hertz-Mindlin para determinar as interações partícula-partícula e partícula-parede, e um modelo de força externa formulado adaptando equações da literatura para descrever as interações partícula-fluido.

Antes de iniciar as simulações, as partículas foram geradas de forma aleatória e homogênea em um volume de análise cilíndrico. O tempo de término da simulação foi calculado como três vezes o tempo de processamento dado por um modelo da literatura. Após o término da simulação, as informações sobre o comportamento do sistema transiente, incluindo posições, velocidades e diâmetros das partículas foram extraídos para análise posterior, que inclui a determinação do tempo de processamento, espessura, e a densidade relativa e a distribuição de tamanho de partícula ao longo da seção transversal do tubo verde.

Os resultados das simulações foram validados com resultados obtidos através de equações apresentadas na literatura. Várias suspensões contendo partículas de tamanho único foram giradas na mesma velocidade de rotação para diferentes diâmetros de partícula e frações de volume de sólido. A densidade relativa final necessária para resolver as equações da literatura foi determinada a partir das simulações.

A partir deste ponto, os parâmetros de manufatura escolhidos para este estudo foram a distribuição de tamanho de partícula do pó de partida, a fração de volume de sólidos na suspensão inicial e a velocidade de rotação. Posteriormente, três níveis foram escolhidos para cada parâmetro, e o método robusto desenvolvido por Taguchi foi selecionado para o planejamento dos experimentos. Os estudos de caso foram definidos usando uma matriz ortogonal L9 (3^4). As respostas para o tempo de formação, a espessura, a densidade relativa e a distribuição de tamanho de partícula ao longo da seção transversal foram avaliadas por meio da análise da resposta média. Além disso, análises adicionais da relação sinal-ruído usando equações do tipo *nominal-the-best* foram realizadas para avaliar a variabilidade em torno do valor médio de alguns parâmetros.

Adicionalmente, misturas de pós de alumina e níquel com diferentes tamanhos e densidades médias de partículas foram utilizadas para compreender o arranjo das partículas durante a centrifugação. Aqui, três abordagens diferentes foram consideradas:
(1) uma suspensão contendo dois pós de alumina com diâmetros médios de partícula que diferem em uma ordem de grandeza;
(2) uma suspensão contendo pós de alumina e níquel com o mesmo diâmetro médio de partícula;
(3) uma suspensão contendo pós de alumina e níquel com diâmetros médios de partícula que diferem em uma ordem de grandeza.

Os valores de entrada necessários para esses experimentos foram escolhidos de acordo com as condições de maior variabilidade da distribuição de tamanho de partícula na seção transversal do tubo verde definidas pelo planejamento de Taguchi.

Finalmente, foram utilizadas combinações de pós de alumina com titania, ytrria estabilizada com zircônia, e níquel para reproduzir experimentalmente as condições das simulações 1, 2, e 3, respectivamente. Para comparar os resultados dos experimentos com as simulações, a microestrutura e mapeamento de elementos das amostras dos tubos verdes foram analisados por microscopia eletrônica de varredura combinada com espectroscopia dispersiva de energia.

Resultados e discussão
A comparação entre os resultados dos estudos de caso *in silico* e os resultados das equações da literatura são dados para o tempo de formação e a espessura do tubo verde. Os resultados do tempo de formação apresentam valores inferiores aos esperados, mas este comportamento

pode ser explicado pelas simplificações do modelo. Já os valores de espessura obtidos nas simulações se aproximam dos valores previstos pelas equações.

A análise da resposta média para o tempo de formação do tubo mostra que os parâmetros de fabricação com maior efeito sobre essa variável são a velocidade de rotação e o diâmetro médio das partículas. A carga de sólidos na suspensão inicial tem uma influência significativamente menor sobre o resultado.

A espessura média do tubo verde depende principalmente da carga do sólido na suspensão, e os outros parâmetros parecem ter um efeito desprezível sobre esta variável. Além disso, a análise da variabilidade da espessura –ou circularidade– da superfície interna mostra que é necessário o uso de pequenas partículas com distribuições de tamanho estreitas, e altas velocidades de rotação para obter um tubo mais arredondado.

Ao longo da seção transversal do tubo, a densidade relativa aumenta das regiões interna para externa para todos os parâmetros, e aumenta de forma geral com a velocidade de rotação. As partículas localizadas perto da parede são conduzidas mais rapidamente por forças mais fortes no sentido da parede, e são pressionadas umas contra outras por camadas e camadas de sólidos, originando uma estrutura mais compacta nas regiões externas. Observa-se também que as regiões de contorno (interna e externa) estão sujeitas a variações devido a mudanças nas variáveis de entrada, enquanto as outras regiões apresentam variações menores.

Apenas a distribuição do tamanho de partícula tem um efeito insignificante sobre a variabilidade da densidade relativa, enquanto as outras variáveis afetam consideravelmente a homogeneidade entre as regiões. Uma suspensão preparada com partículas pequenas e uma carga elevada de sólidos, submetida a uma alta velocidade de rotação deverá produzir à maior homogeneidade em termos de densidade relativa.

A análise da distribuição do tamanho de partícula para a suspensão depois da centrifugação mostra que partículas menores são predominantes na fase após o processo. Por outro lado, a seção transversal do tubo verde não parece sofrer tanta variação quanto à suspensão. Variações significativas são observadas na distribuição do tamanho das partículas através da análise da relação sinal-ruído devido ao diâmetro médio da partícula do pó inicial e sua distribuição de tamanho, mas os valores brutos indicam que a distribuição das partículas é semelhante à distribuição da mistura de partículas original.

Os testes adicionais formulados para misturas de pós mostram que a segregação por tamanho das partículas é desprezível, exceto para diferenças de tamanho acima de uma ordem de grandeza. A segregação devido à densidade também foi observada, mas as diferenças de tamanho podem facilmente ofuscar seu efeito, conforme confirmado por meio de trabalhos experimentais.

Considerações finais

O *centrifugal casting* é uma técnica ideal para obter materiais com gradiente funcional de forma simples e direta para diversas aplicações, como manufatura de membranas cerâmicas. As diferenças de densidade podem ser exploradas para obter perfis de composição, mas esses perfis dependem também da diferença de tamanho entre os pós. Portanto, ambos os parâmetros devem ser ajustados conjuntamente para obter o resultado desejado.

Palavras-chave: Centrifugal casting. Método de elementos discretos. Planejamento robusto. Segregação por tamanho. Material com gradiente funcional.

ABSTRACT

Centrifugal casting is a shaping technique intended for ceramic tubular structures manufacture, where the particle size and density are exploited to produce functionally graded materials and asymmetrical membranes. However, some well-established insights about the segregation phenomena are debatable and remain unclear. For instance, small particles do not necessarily stay in the inner region, and the bigger particles do not accumulate in the outer. Herein several manufacturing parameters were studied through Taguchi's robust design, using a discrete element method-based simulation to generate the data. Alumina and nickel powders were used as model materials, assessing the green cast formation time, the cast thickness, the roundness, and also the changes in relative density, and particle size distribution along the cast's cross-section. The mean particle diameter and the rotation speed are the most influential parameters for the casting time. The volume fraction of solids on the precursor slurry is decisive regarding the cast structural properties, and particle segregation is negligible, excepting for size differences above one order of magnitude. Density segregation was also observed, but the size differences can easily overshadow its effect, as confirmed through experimental work.

Keywords: Centrifugal casting. Discrete element method. Robust design. Size segregation. Functionally graded materials.

LIST OF FIGURES

LIST OF TABLES

LIST OF ABBREVIATIONS

CFD   Computational Fluid Dynamics

DEM   Discrete Element Method

EDS   Energy Dispersive Spectroscopy

PSD   Particle Size Distribution

SEM   Scanning Electron Microscopy

SNR   Signal-to-Noise ratio

YSZ   Yttria Stabilized Zirconia

SUMMARY

1 INTRODUCTION

1.1 CONTEXTUALIZATION

Ceramic membranes have gained relevance in the last few decades in membrane separation processes due to their high chemical, thermal and mechanical stabilities. Their applications include water and wastewater treatment, food and beverage processing, chemical and pharmaceutical processing, gas separation, and purification operations (DRIOLI; GIORNO, 2016; GITIS; ROTHENBERG, 2016).

The manufacture of ceramic membranes usually involves a large number of stages. These stages are carried out under conditions that ultimately alter the structure and the properties of the final product. Understanding each manufacturing condition's influence over the outcome can lead to obtaining the most suitable membrane for a specific application (GUAN et al., 2016).

In general, ceramic membranes are asymmetric hierarchical structures divided into a dense or slightly porous selective layer that determines separation properties, a highly porous support layer that provides mechanical strength to the structure, and an intermediate layer that bonds the previous two together. The support layer is commonly manufactured following three steps: formation of the slurry, shaping the green cast, and sintering (ISSAOUI; LIMOUSY, 2019; LI, 2007).

Here, the shaping step can differ depending on the desired geometry. In tubular support manufacturing, some shaping techniques include extrusion and centrifugal casting. Extrusion is the most popular one. However, the green tubes shaped by centrifugal casting can offer a more homogeneous structure with a rounder and smoother inner surface. Hence, green tubes obtained by centrifugal casting are considered of higher quality for further sintering and ultimately coating with the remaining layers (BERTOTTO et al., 2019; HARABI; BOUZERARA; CONDOM, 2009).

Besides, this method allows the formation of a hierarchical structure since the green tubes can have a graded porosity, hence a different pore size distribution, along the cross-section (CARO, 2016). Depending on manufacturing conditions, both the support and the intermediate layers could be manufactured at once, seemingly reducing membrane manufacture cost (NUNES et al., 2020).

Despite previous efforts, the knowledge about centrifugal casting is insufficient to forecast the correct trends given by a set of manufacturing conditions regarding the particle and density segregation phenomena concerning the green cast structure. In this work, we investigate the influence of processing parameters assessing the particle and density segregation and its relation with the cast relative density, using a DEM-based simulation approach combined with robust design.

1.2 OBJECTIVES

1.2.1 General objective

The main objective of this work is to contribute to the research field of centrifugal casting for ceramic membranes manufacture, identifying key parameters of the process and their effect on the green cast's structure.

1.2.2 Specific objectives

In order to reach the main goal, the following steps were defined:

- Validate an adapted DEM-based simulation tool using information from the literature to represent systems during centrifugal casting.
- Evaluate the effect of selected parameters on the manufacture of tubular structures by a robust design of experiments.
- Assess particle segregation along the cast's cross-section due to particle size and density.
- Perform bench experiments to verify the results from the simulations.

2 LITERATURE REVIEW

2.1 CENTRIFUGAL CASTING

Centrifugal casting consists of the rotation of a ceramic slurry inside a cylindrical mold around its axis. The generated centrifugal force field induces the separation of the components based primarily on a density difference, i.e., the solids concentrate towards the mold wall. The lower density phase remains close to the center of the tube. After this, the separated liquid is drained, and the green tube is removed from the mold for further treatment (BIESHEUVEL; NIJMEIJER; VERWEIJ, 1998).

2.2 MODELLING AND SIMULATION

2.2.1 Continuum approach

Some effort has been made to describe the centrifugal casting process theoretically. For instance, Biesheuvel et al. (1998) developed equations for the unhindered and the hindered settling of monosized particles with equal densities from a continuum approach. They described the cast formation in a vertical cylindrical mold neglecting the diffusion of the solid from the cast to the suspension phase and the effect of gravity force. They ultimately derived an expression to predict the final cast thickness from an overall mass balance, used mass transport equations to evaluate the cast thickness' evolution over time for several conditions, and compared their results with experimental results.

Moreover, Biesheuvel et al. (2001) developed a model to predict the particle size distribution along the green cast's cross-section after centrifugation. For a constant final porosity and laminar flow, they estimated the average particle diameter in several layers of the cast starting from a defined particle size distribution. They showed that the fraction of particles of every size in each layer of the cast is barely equal only under a set of conditions, except for the inner layer in which the smallest particles prevail.

2.2.2 Discrete approach

An alternative approach has been proposed applying the Discrete Element Method (DEM), which has been widely used to describe particulate systems. In DEM, the modeled particles are assumed to be individual entities using a Lagrangian scheme for which a balance of forces is established to obtain information such as position or velocity over time. The system's overall behavior is determined through particle-particle and particle-wall interactions which are described using specific contact models (CUNDALL; STRACK, 1979). The interaction between particle and fluid can be considered by coupling Computational Fluid Dynamics (CFD) models into the calculations (KIECKHEFEN et al., 2020) or introducing the forces acting over the particles directly into the forces' balance.

The latter methodology has been used by Hong (1996, 1997a) to develop a tool to simulate centrifugal casting coupling the DLVO theory on long-range particle interactions, JKR adhesion model, and Hertz-Mindlin contact model to DEM equations. Hong (1997b) performed *in silico* centrifugal casting tests through dynamic similarity to analyze particles' rearrangement during the casting for several solids volume fractions in a rectangular box. Limiting to the smallest particles on the suspension seems that the particles migrate slower into the cast structure than other particles for all solid loadings, in agreement with Biesheuvel et al. (2001), but the behavior of the particles of other sizes was not evaluated to infer that significant segregation by size occurs.

2.3 EXPERIMENTAL STUDIES

Additionally, many experimental studies have been performed to assess the influence of various parameters such as particle mean diameter and rotation speed over the tube's properties after sintering (BISSETT; ZAH; KRIEG, 2008; KIM et al., 2002; STEENKAMP et al., 2001). However, only a handful focuses on the effects of the structure of the green cast. Nijmeijer et al. (1998) studied the rotation speeds and the processing time's influence over the green cast's thickness and total porosity. While increasing both inputs has the same effect on the thickness, the influence over the total porosity remains unclear. Falamaki and Veysizadeh (2008) investigated the influence of rotation speed, mold volume, pH, and binder content in flat disc membrane manufacture. Even though the changes in rotation speed and pH seemed to

alter the porosity and the pore diameter on the top surface, binder concentration had a much higher effect over those outputs and they were estimated after sintering.

3 METHODOLOGY

3.1 SIMULATION AND DATA PROCESSING

The centrifugal casting process was performed *in silico* using an open-source DEM simulation framework MUSEN (DOSTA; ANTONYUK; HEINRICH, 2013; DOSTA; SKORYCH, 2020). The initial system (Figure 1) consists of an aqueous α-alumina slurry, rotated horizontally around the y-axis in a stainless steel 304 cylindrical mold of 2.5 mm of internal radius r_{mold}. The mold was centered at the system's origin. The z-axis was considered as the vertical axis, in which gravity force acts downwards over the system.
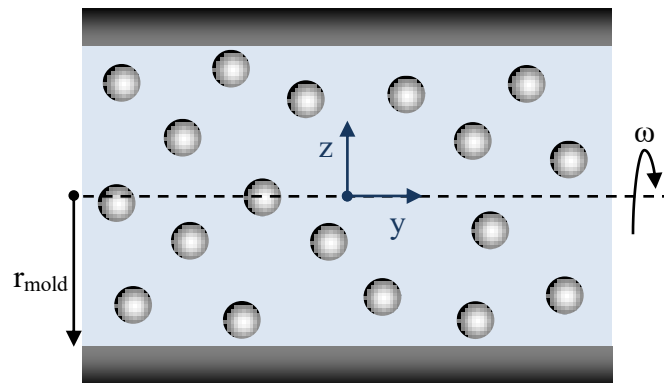
Figure 1 − Schematic representation of the system.

For particle-particle and particle-wall interactions, the Hertz-Mindlin contact model (HERTZ, 1882; TSUJI; TANAKA; ISHIDA, 1992) has been incorporated. The required properties for pure solid materials are listed in Table 1. Meanwhile, for pairs of materials, the restitution coefficient is 0.6, and the sliding and rolling friction coefficients are 0.1 and 0.01, respectively.

Table 1 – Physical and mechanical properties for pure materials.

Property	α-alumina	Stainless steel 304
Density ($kg \cdot m^{-3}$)	3950	7901
Young's modulus (GPa)	370	193
Poisson ratio (-)	0.22	0.29

Fonte: CARDARELLI (2018).

An external force model was incorporated, adapting equations from Biesheuvel et al. (1998) to describe particle-fluid interactions. For each particle, it was assumed that the movement of a single spherical particle through a fluid phase under the influence of a centrifugal force field is given by a combination of friction, $\mathbf{F_f}$ (Eq. 1), centrifugal force and buoyancy, $\mathbf{F_{c+b}}$ (Eq. 2a,b,c). Here, r_p, m_p, V_p and $\mathbf{v_p}$ are radius, mass, volume, and velocity of particle; μ, ρ_l and $\mathbf{v_l}$ are viscosity, density, and velocity of the fluid phase; $c_{p,x}$ and $c_{p,z}$ indicate the position at the center of the particle; and ω is the mold's rotation speed (or angular velocity) around the y-axis. Bold characters represent vectors. For all calculations, water at room temperature was considered as the fluid phase. The respective density and viscosity of the fluid were equal to 997.1 kg·m^{-3} and 8.905×10^{-4} Pa·s (BELL et al., 2014).

$$\mathbf{F_f} = 6\,\pi\,\mu\,r_p\left(\mathbf{v_l} - \mathbf{v_p}\right) \tag{1}$$

$$F_{c+b,x} = \left(m_p - V_p\,\rho_l\right)c_{p,x}\,\omega^2 \tag{2a}$$

$$F_{c+b,y} = 0 \tag{2b}$$

$$F_{c+b,z} = \left(m_p - V_p\,\rho_l\right)c_{p,z}\,\omega^2 \tag{2c}$$

Before starting the simulations, the particles were randomly and homogeneously generated into a cylindrical analysis volume, situated inside the mold, whose radius equals the mold's internal radius. The length of analysis volume is ten times the largest particle diameter defined for the test, and its lids were defined as periodic boundaries over the y axis. The number of generated particles changes depending on the different initial conditions. It depends on the particle size distribution and the volume fraction of solids in the suspension.

Furthermore, it has been assumed that the liquid phase follows the mold's motion from the starting point, and the particles are dragged by the motion of the liquid and gain its velocity. Thus, to generate consistent initial conditions, the particles' initial velocity is defined depending on their position (Eq. 3a,b,c).

$$v_{p,x} = c_{p,z}\,\omega \tag{3a}$$

$$v_{p,y} = 0 \tag{3b}$$

$$v_{p,z} = -\,c_{p,x}\,\omega \tag{3c}$$

The simulation time step was adopted based on the Rayleigh time for each configuration. In order to obtain appropriate information about system behavior the simulation results were saved every 1×10^{-3} s. The end time was calculated as three times the casting time given by the model for unhindered settling by Biesheuvel et al. (1998). After the simulation ends, the complete information about transient system behavior including positions, velocities and diameters of particles were extracted for further analysis.

The particle coordinates for all time steps saved were transformed from Cartesian (x,y,z) to cylindrical (ρ,φ,y) coordinates for simplification to begin estimating the cast formation time and the final cast thickness. The system was divided into quadrants of the plane ρ-φ, as seen in Figure 2, and the cast thickness $\delta_{i,j}$ was calculated in each quadrant i for all time points saved j (Eq. 4). Then, the mean cast thickness δ_j was calculated for a specific time point j (Eq. 5).
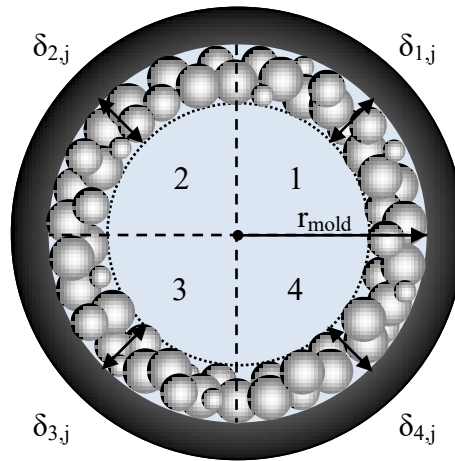
Figure 2 – Frontal view (plane ρ-φ) of the division of the system in quadrants for cast thickness estimation in an instant time point j.

$$\delta_{i,j} = r_{mold} - \left(\rho_{min,i,j} - r_{min,i,j}\right) \tag{4}$$

$$\overline{\delta}_j = \frac{\sum \delta_{i,j}}{4} \tag{5}$$

Here, $\rho_{min,i,j}$ and $r_{min,i,j}$ are the radial position and the particle's radius with the minimum distance to the mold's center. A cut-off was implemented to avoid overestimating values due to irregularities during particle settling, excluding 0.5% of closest particles inside the quadrant.

The mean cast thickness values obtained for all time points saved were used to estimate transient behavior. The cast formation time was defined as the time point for which the relative deviation of the mean thicknesses $E_{r,j}$ (Eq. 6) between consecutive time points fell under 0.1%. Consequently, the final cast thickness $\bar{\delta}$, or the green cast's thickness, was defined as the value corresponding to the cast formation time, and all subsequent parameters have been estimated for this instant.

$$E_{r,j} = \frac{\left|\bar{\bar{\delta}}_{j-1} - \bar{\delta}_j\right|}{\bar{\bar{\delta}}_{j-1}} \times 100 \tag{6}$$

Afterward, the green cast's cross-section was divided into five annular cylindrical regions of thickness equal to 20% of the final cast thickness to perform the relative density estimations, as shown in Figure 3. There were added cuts into the inner (1) and the outer (5) regions of a thickness equal to the radius of the mean-sized particle of the test, $r_{p,mean}$, to avoid underestimations due to boundary effects. Then, the relative density in region k is calculated as the ratio of the volume of solids inside the region k to the total volume of the region k. Here, the volume of solids is the sum of all whole particles' volumes and particle caps which are located on the boundaries of the region k. The total volume of the region k is the annular cylinder's volume that sets the region's boundaries.
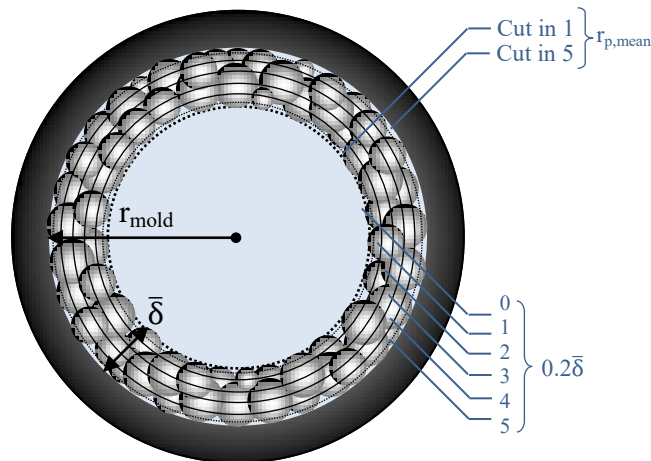

Figure 3 − Frontal view (plane ρ-φ) of the division of the system in regions for relative density estimation.

Lastly, the particle size distribution (PSD) over the cross-section was evaluated using the same division of regions as the relative density estimations but disregarding the cuts in the

inner and outer regions. The suspension phase region (0) was added to evaluate the distribution of the particles that remained in suspension after casting. For this purpose, the particles were classified according to their positions into six classes. For each class a mean particle diameter $d_{p,k}$ was calculated number-based taking into account only the particles located in the specific region.

To better understand segregation effects occurring in the process the deviation of the mean diameters $d_{p,k}$ from the mean diameter of the original powder $d_{p,mean}$ was calculated. The results were normalized to obtain $d_{p,k}^{*}$ dividing by the difference between the maximum $d_{p,max}$ and the mean $d_{p,mean}$ particle diameters of the original powder (Eq. 7), leaving the values in a range of [-1; 1]. The normalization allowed the efficient analysis of segregation effects since negative values indicate the smaller particles of the system predominate, and positive values indicate that bigger particles prevail. Values equal to zero show that the proportion is balanced within the region.

$$d_{p,k}^{*} = \frac{d_{p,k} - d_{p,mean}}{d_{p,max} - d_{p,mean}} \tag{7}$$

3.2 VALIDATION

The results from the simulations and data processing were compared with results obtained from the equations derived by Biesheuvel et al. (1998). This was done for the unhindered and the hindered settling of monosized particles for complete mold filling and from an equation derived through an overall mass balance. The cast formation time and the final cast thickness were determined for the same input parameters and variables as the simulations.

Several suspensions containing monosized particles were rotated at 500 rad·s^{-1} for different particle diameters and volume fractions of solid, as detailed in Table 2. As for the final relative density required to solve the equations from the literature, they were extracted from the simulations. All *in silico* case studies were performed in duplicate.

Table 2 – Case studies proposed for comparison with equations from the literature.

Case study	Particle diameter (mm)	Volume fraction of solid (–)
A1	0.050	0.15
A2	0.050	0.25
A3	0.100	0.15
A4	0.100	0.25

3.3 EVALUATION OF MANUFACTURING PARAMETERS THROUGH ROBUST DESIGN

The manufacturing parameters chosen for this study were the particle size distribution (PSD) of the starting powder, the volume fraction of solids in the initial suspension, and the rotation speed. The PSD of initial powder's was defined as a normal distribution with mean μ –or particle mean diameter $d_{p,mean}$– and standard deviation σ. The PSD was defined in the discretized form and represented with five size classes. The interval of the distribution was set as [μ − 0.02 mm; μ + 0.02 mm], i.e., there were considered five sizes with a difference of 0.01 mm among them for all means studied. The fraction σ/μ defines the proportion of each particle size into the powder, and the proportions for the fractions considered in this work are shown in Table 3.

Table 3 – Number fraction of particles of each diameter for a given PSD.

PSD σ/μ (-)	Size class 1 $d_{p,min}$ (%)	Size class 2 (%)	Size class 3 $d_{p,mean}$ (%)	Size class 4 (%)	Size class 5 $d_{p,max}$ (%)
0.2	0.26	16.55	66.38	16.55	0.26
0.3	3.77	23.99	44.48	23.99	3.77
0.4	8.56	24.27	34.34	24.27	8.56

Afterward, three levels were chosen for each parameter, and the robust design method developed by Taguchi (TAGUCHI; CHOWDHURY; WU, 2005) was selected for the design of experiments. The case studies for an L_9 (3^4) orthogonal array are shown in Table 4. All case studies were performed *in silico* in triplicate, and the responses for cast formation time, cast thickness, relative density, and PSD over the cross-section were evaluated by analyzing the average response. For those variables determined in more than one region, additional analyses of the Signal-to-Noise ratio (SNR) using nominal-the-best equations

(TAGUCHI; CHOWDHURY; WU, 2005) were performed to evaluate the variability around the mean value.

Table 4 – Detail of experiments for an L_9 (3^4) orthogonal array.

Case study	Mean diameter (mm)	PSD σ/μ (−)	Volume fraction of solid (−)	Rotation speed (rad/s)
B1	0.050	0.2	0.15	150
B2	0.050	0.3	0.20	300
B3	0.050	0.4	0.25	450
B4	0.075	0.2	0.20	450
B5	0.075	0.3	0.25	150
B6	0.075	0.4	0.15	300
B7	0.100	0.2	0.25	300
B8	0.100	0.3	0.15	450
B9	0.100	0.4	0.20	150

3.4 ASSESSMENT OF PARTICLE SEGREGATION ALONG THE CAST'S CROSS-SECTION

To fully comprehend the particle rearrangement after centrifugation, additional *in silico* tests were carried out using mixtures of powders with different mean particle sizes and densities. Here, three different approaches were performed:

- a suspension containing two α-alumina powders with mean particle diameters that differ in one order of magnitude;
- a suspension containing α-alumina and nickel powders with the same mean particle diameter;
- a suspension containing α-alumina and nickel powders with mean particle diameters that differ in one order of magnitude.

Nickel's density, Young's modulus and Poisson ratio are 8900 kg·m^{-3}, 207 GPa and 0.31, respectively (CARDARELLI, 2018), whereas other properties remain unchanged. The input values required for these experiments were chosen in agreement with the SNR analysis for the particle size distribution over the cross-section's variability. All the case studies were performed in triplicate.

3.5 EXPERIMENTAL

A few bench experiments were performed in order to corroborate the findings from the *in silico* ones. For this purpose, alumina (CT3000SG, Almatis), yttria stabilized zirconia (YSZ) (Zirconium(IV) oxide-yttria stabilized with 8 mol.% Y_2O_3, Sigma Aldrich), titania (Aeroxide TiO_2 P25, Evonik), and nickel (Epson Atmix Corporation) powders were chosen to be used as raw materials for the experiments based on the setup proposed in section 3.4. Their purities are above 99 % and their main properties are given in Table 5. These powders were mixed with distilled water to prepare the slurries. No dispersing agent, binder or other additives were added.

Table 5 – Powder's main properties.

Material	Median diameter (µm)	Density (kg·m^{-3})
Alumina	0.500	3950
YSZ	0.700	6045
Titania	0.025	4240
Nickel	6.000	8900

The slurries were prepared by mixing 25 vol.% solids and 75 vol.% distilled water. The solids' mixtures used in this work are detailed in Table 6. The slurries were stirred using a mechanic stirrer for 30 min at room temperature. Then they were poured into stainless steel 304 molds, with 1 cm of internal diameter and 15 cm of length, previously coated with vaseline, and hermetically closed for shaping using the centrifugal casting technique. The filled molds were horizontally rotated at 450 rad·s^{-1} for 10 min, except the ones containing titania which were rotated for 40 min, using the equipment shown in Figure 4. After rotation, the remaining suspension was drained and the green casts were dried inside the molds in a drying chamber at room temperature (approximately 25°C) and relative humidity of 70 % for 3 days.

The microstructure (inner, outer, and fractured cross-section surfaces) and element mapping (inner and outer surfaces) of the green tubes' samples were analyzed by scanning electron microscopy (SEM) combined with energy dispersive spectroscopy (EDS) in a JEOL JSM 6390LV scanning electron microscope after coating with gold.

Table 6 ‒ Powder mixtures for slurries preparation (dry basis).

Powder mixtures		Volume fraction (‒)		Mass fraction (‒)	
Powder 1	Powder 2	Powder 1	Powder 2	Powder 1	Powder 2
Alumina	–	1	–	1	–
Alumina	YSZ	0.9	0.1	0.855	0.145
Alumina	Titania	0.9	0.1	0.893	0.107
Alumina	Nickel	0.9	0.1	0.800	0.200
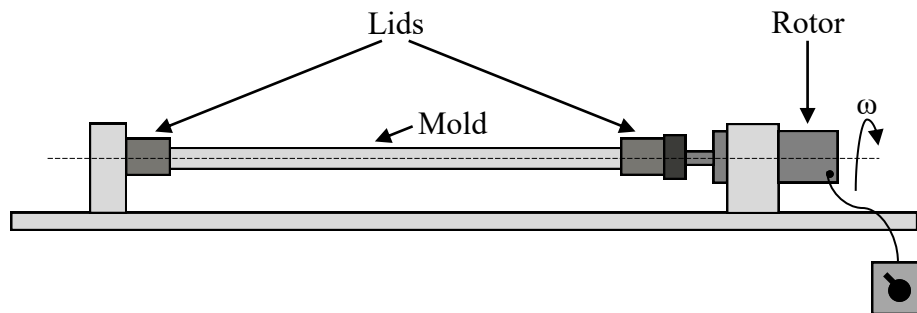
Figure 4 ‒ Schematic representation of the experimental equipment.

4 RESULTS AND DISCUSSION

4.1 VALIDATION

The simulation results for the case studies defined in Table 2 are provided in Table 7. The relative density values observed in Table 7 are typical for centrifugal casting samples before sintering (BIESHEUVEL; NIJMEIJER; VERWEIJ, 1998; FALAMAKI; VEYSIZADEH, 2008; NIJMEIJER et al., 1998). The mean overall relative density value estimated from the simulations was 0.506, and its standard deviation was 0.027. As afore-mentioned, the mean was taken to solve the literature's equations.

Table 7 – Results from simulations performed for validation.

Case study	Number of particles	Cast formation time (s)	Cast thickness (mm)	Relative density (−)
A1	22500	0.014 ± 0.000	0.400 ± 0.000	0.510 ± 0.000
A2	37500	0.013 ± 0.000	0.670 ± 0.004	0.538 ± 0.003
A3	5625	0.010 ± 0.001	0.439 ± 0.009	0.469 ± 0.009
A4	9375	0.009 ± 0.000	0.718 ± 0.004	0.508 ± 0.002

The comparison among the cast formation time results from the *in silico* case studies and the results from the literature's equations can be observed in Figure 5, and the comparison for the cast thickness is shown in Figure 6. The cast formation time results indicate that the time values decrease when the particle diameter increases, while the volume fraction of solids on the initial suspension barely affects the results. These tendencies are in agreement with Biesheuvel et al.'s observations (1998).

In general, the time values obtained for the unhindered settling model are lower than the time values obtained for the hindered model, which is reasonable because the former disregards the interaction among the particles and its effect on the settling velocity. According to this, the simulations' results were expected to be higher than the unhindered settling times, but this was observed only for the larger particles. One of the reasons is that we assumed that the fluid and the particles have the same velocity as the mold from the beginning of the simulation, even though it will take a small fraction of time for the system to depart from repose and reach this condition. This means that the casting time could be underestimated. Despite this, the results are all of the same order of magnitude.
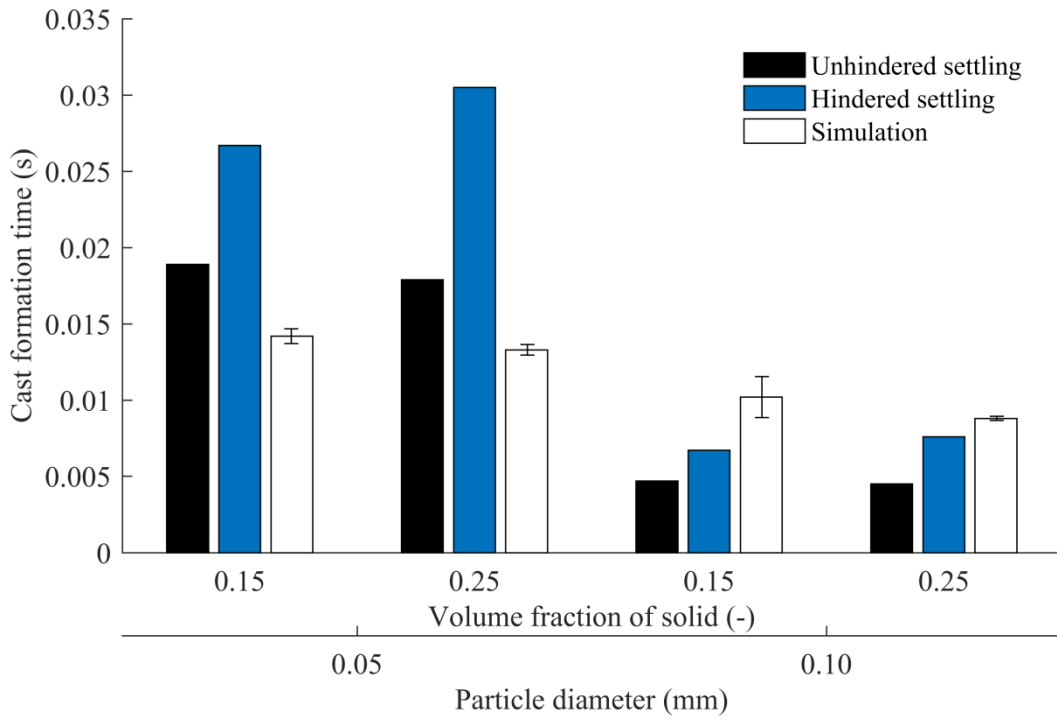
Figure 5 – Cast formation time results of models from the literature and simulations.
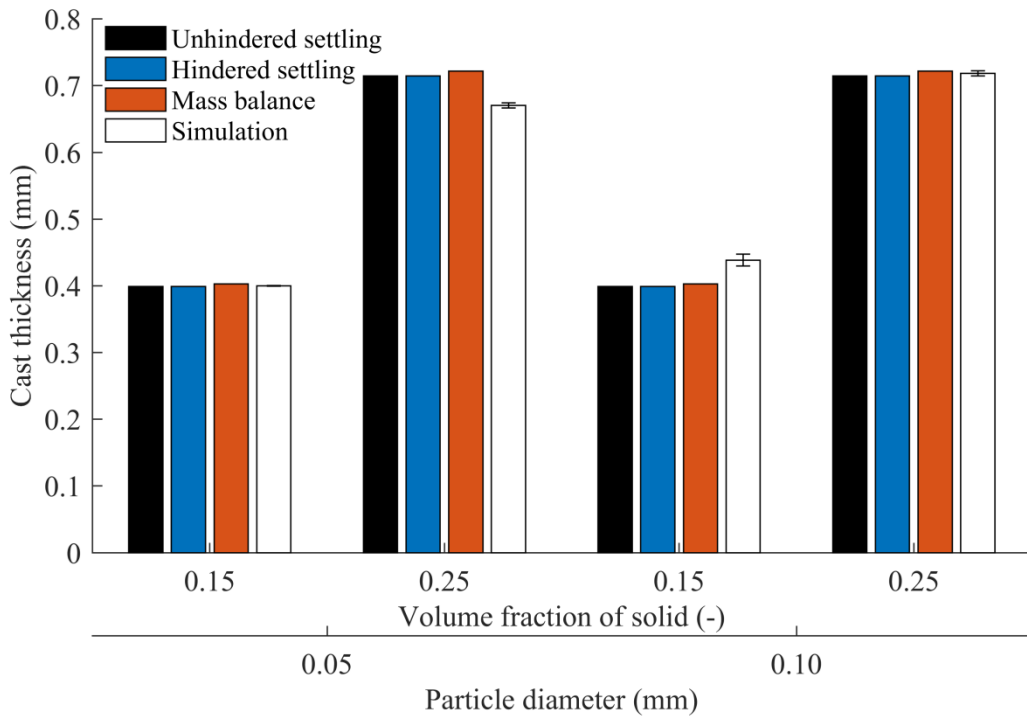

Figure 6 – Cast thickness results of models from the literature and simulations.

Meanwhile, the green cast thickness (Figure 6) increases with the volume fraction of solids in the initial suspension. However it does not influenced by the particle diameter, that also in agreement with Biesheuvel et al. (1998). The unhindered and the hindered models are equal and correspond to 99% of the ideal result given by the equation derived from an overall mass balance. The values obtained through the simulations are close to the values predicted by the equations.

4.2 EVALUATION OF MANUFACTURING PARAMETERS THROUGH ROBUST DESIGN

The simulation results for the case studies defined in Table 4 are summarized in Table 8. The analyses of average response for the cast formation time and the mean cast thickness can be observed in Figure 7 and Figure 8, respectively. The analysis of variability among the quadrants of the latter is shown in Figure 9. Herein, in all figures, a solid line represents the mean value $\bar{x}$, and dotted lines representing the limits of the confidence interval at the 95% confidence level for every set of samples.
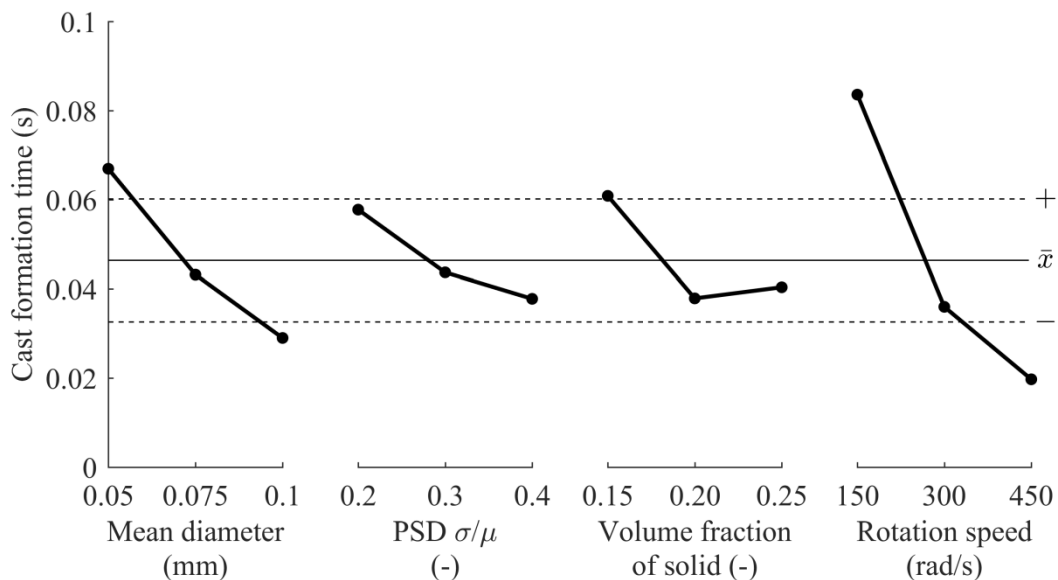

Figure 7 – Average response analysis of the cast formation time.

Table 8 – Results from robust design of experiments.

Variable	Case study									Statistics		
	B1	B2	B3	B4	B5	B6	B7	B8	B9	$-^*$	$\bar{x}$	$+^*$
Number of particles	30221	38399	46032	16576	20264	11920	11130	6593	8691	-	-	-
Cast formation time (s)	0.130	0.045	0.026	0.019	0.072	0.039	0.024	0.014	0.049	0.033	0.046	0.060
Mean cast thickness (mm)	0.419	0.526	0.649	0.539	0.708	0.422	0.704	0.438	0.591	0.511	0.555	0.599
SNR for thickness variability (dB)	31.904	40.465	33.812	36.026	28.241	29.459	32.431	30.977	24.889	30.014	32.023	34.031
Relative density in 1 (−)	0.218	0.394	0.482	0.388	0.327	0.254	0.382	0.346	0.240	0.302	0.337	0.371
Relative density in 2 (−)	0.556	0.599	0.603	0.593	0.581	0.544	0.585	0.506	0.516	0.551	0.565	0.579
Relative density in 3 (−)	0.591	0.596	0.599	0.593	0.584	0.601	0.589	0.595	0.588	0.591	0.593	0.595
Relative density in 4 (−)	0.587	0.592	0.597	0.593	0.581	0.597	0.587	0.598	0.593	0.589	0.592	0.594
Relative density in 5 (−)	0.611	0.606	0.604	0.609	0.597	0.660	0.596	0.856	0.617	0.608	0.640	0.671
SNR for relative density variability (dB)	9.731	15.714	20.843	15.411	13.225	10.340	15.422	9.789	10.234	11.929	13.412	14.895
$d_{p,0}^{*}$ (−)	-0.339	-0.652	-0.611	-0.042	-0.280	0.194	-0.033	-0.046	-0.171	-0.363	-0.220	-0.077
$d_{p,1}^{*}$ (−)	-0.056	-0.093	-0.083	0.009	-0.035	0.026	0.015	0.095	0.010	-0.036	-0.012	0.011
$d_{p,2}^{*}$ (−)	-0.024	-0.003	0.011	0.002	-0.007	-0.005	-0.002	0.012	0.004	-0.006	-0.001	0.003
$d_{p,3}^{*}$ (−)	0.013	0.034	0.034	-0.001	0.021	0.024	0.001	-0.005	0.015	0.009	0.015	0.021
$d_{p,4}^{*}$ (−)	0.020	0.035	0.036	0.017	0.016	0.006	0.011	0.003	0.017	0.013	0.018	0.023
$d_{p,5}^{*}$ (−)	0.012	-0.010	-0.017	-0.022	-0.013	-0.035	-0.017	-0.020	-0.042	-0.025	-0.018	-0.012
SNR for $d_{p,k}^{*}$ variability (dB)	29.862	25.615	26.162	36.486	32.986	32.986	37.597	26.909	31.306	29.207	30.965	31.722

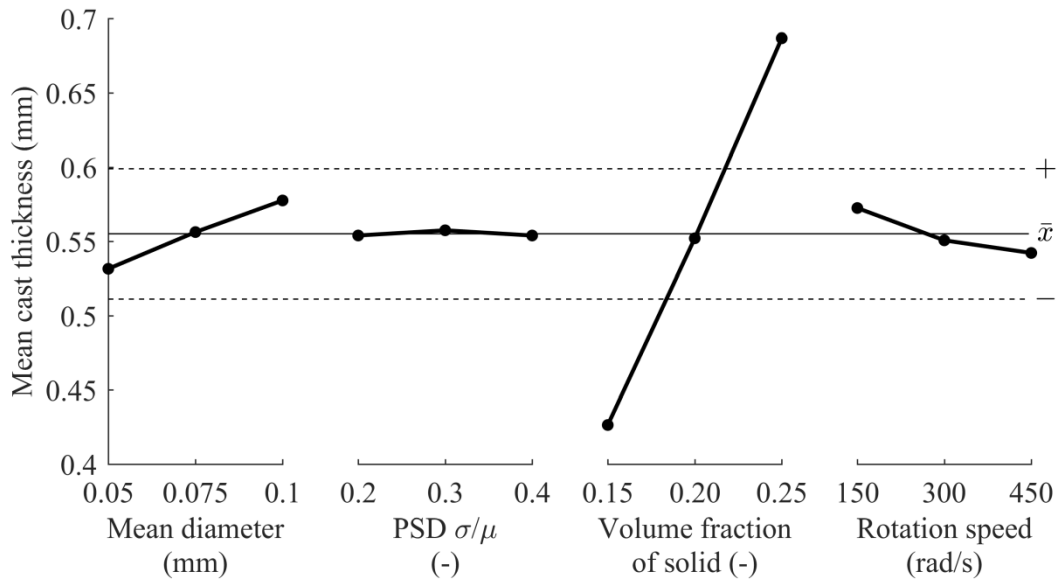*Limits of the interval of confidence at the 95% confidence level.

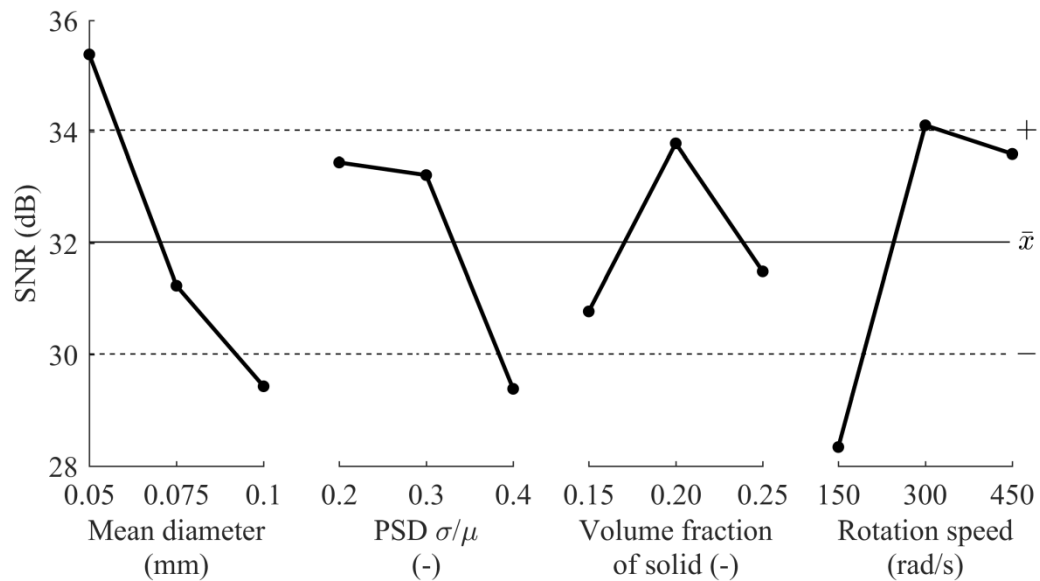Figure 8 – Average response analysis of the mean cast thickness.

Figure 9 – Signal-to-Noise ratio analysis of the cast thickness variability.

According to the average response analysis for the cast formation time observed in Figure 7, the manufacturing parameters with a higher effect over this output variable are the rotation speed, and the particle mean diameter. For both of them, the casting time decreases when the input variable goes up due to their direct and inverse effect on particle settling velocity. Meanwhile, the solid loading on the initial suspension shows the same effect but has a significantly lesser influence over the outcome.

Based on the literature (BIESHEUVEL; NIJMEIJER; VERWEIJ, 1998; FALAMAKI; VEYSIZADEH, 2008; HONG, 1997b), the effect of manufacturing parameters over the mean cast thickness depends mainly on the solid loading. The analysis of the means confirms this effect, where the thickness increases rapidly with the solid volume fraction, and other parameters seem to have a negligible effect over this variable.

Additionally, the variability of the thickness –or roundness– of the inner surface can be evaluated by taking the cast thickness values obtained per quadrant, defined in Figure 2, previously used to get the mean value. The SNR analysis performed to those values (Figure 9) shows that the particles' mean diameter, their size distribution and the system's rotation speed significantly influence the green cast roundness.

High SNR values indicate lower variations and low SNR values indicate higher variations among data. Keeping this in mind, we can expect that the lowest particle size and an intermediate rotation speed would lead to the highest SNR for all experiments, and the lowest SNR would be found with a combination of high particle size with wide distribution and low rotation speed. These setups correspond to case studies B2 and B9 (Table 4), respectively, and their SNR values, listed in Table 8, agree with the expected behavior. Therefore, it can be inferred that it is necessary to use small particles with narrow size distributions and high rotation velocities to minimize the thickness variability, thus obtaining a higher roundness, to obtain an improved finish for further sintering.

The relative density's behavior across the green cast's cross-section is analyzed through Figure 10 and Table 8. At first glance, it can be noticed that the relative density increases from inner (1) to outer (5) regions for all parameters. The inner region (1), which represents 20% of the green cast's thickness, has the lowest relative density values while the other regions exhibit similar but increasing values. This has been reported previously by Chang et al. (1991), who observed a looser structure on the region closest to the center of rotation and a more compact body near the wall.

The system's rotation is responsible for the generation of a centrifugal force field, which strongly affects the net force that leads to particles' motion. Since the centrifugal force depends on the radial position, the particles are subject to a force gradient that goes from zero at the center of the tube to a maximum value near the mold. Hence, at the beginning of the process, there is established a velocity profile with the same characteristics. The particles located near the wall are driven faster by stronger forces to the wall and are pressed against each other by layers and layers of solid, originating a more compact structure in the outer

regions. However, this effect does not occur with the particles that arrive last to the cast, forming the inner region, because they are subject to weaker forces. This phenomenon can also explain the overall increase in relative density observed in Figure 10 when the rotation speed increases.
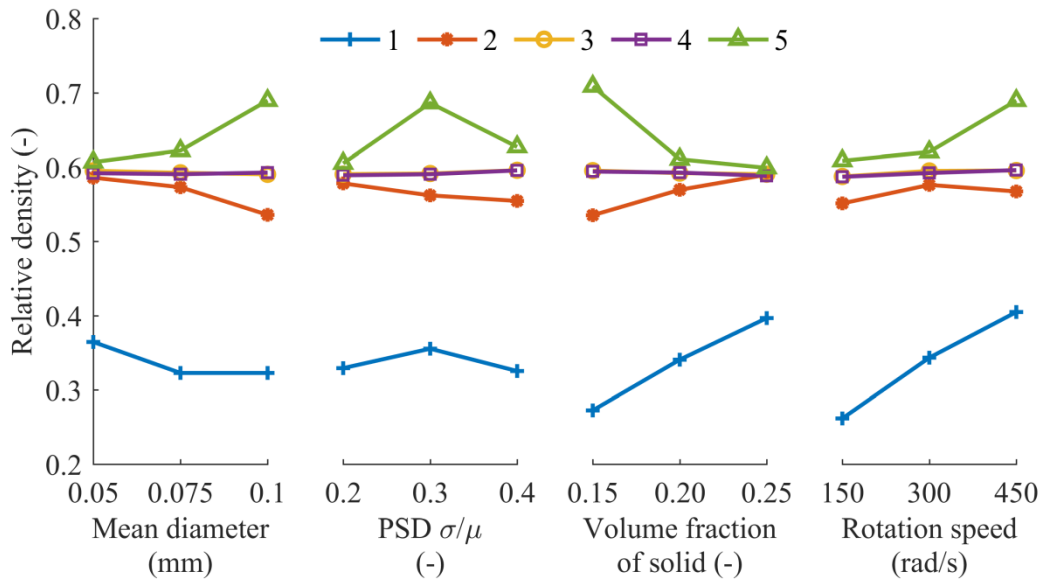

Figure 10 − Analyses of average response for the relative density over the green cast's cross-section from the inner (1) to outer (5) regions.

In addition, Figure 10 shows that the boundary regions (1 and 5) are prone to variations due to changes in the input variables whereas the internal regions (2, 3, and 4) exhibit lower variations, being negligible for the last two. According to the values and the statistics provided in Table 8, the inner region (1) is more susceptible to variations in solid's volume fraction and rotation speed. Here, the increase in both input parameters leads to a significant increase in the relative density. On the other hand, the outer region (5) suffers significant changes for all process parameters. In this case, the increase in the solid's volume fraction leads to a decrease in the relative density while the tendency for the rotation speed remains the same as region (1). Suspensions with bigger particles seem to produce a denser outer layer and the effect of the size distribution is not clear from this first assessment.

The relative density's variability over the cross-section can be analyzed in Figure 11. Only the particle size distribution has a negligible effect over the variability, while the other variables considerably affect the relative density's homogeneity over the regions, as expected from Figure 10.
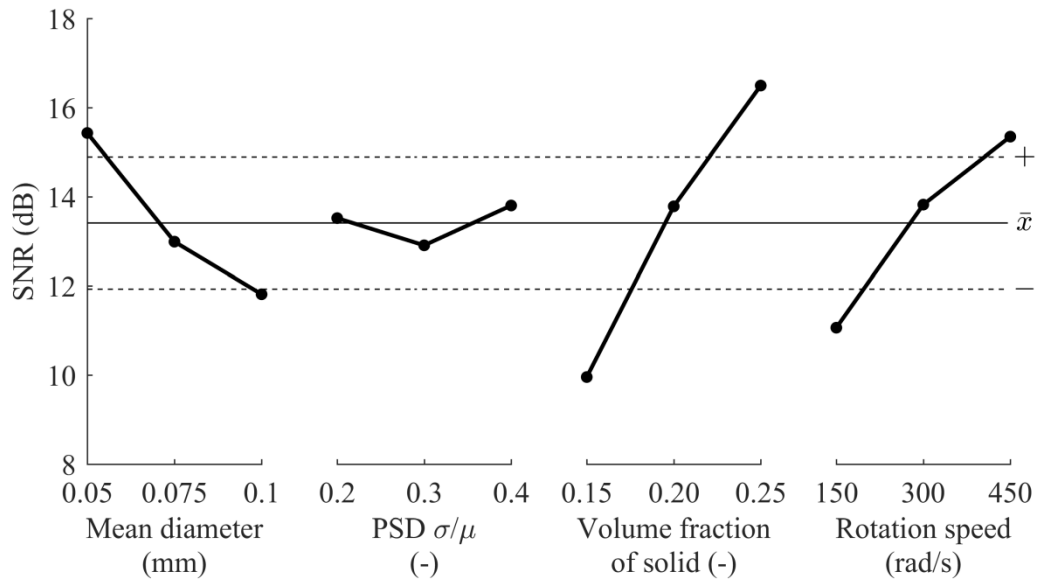
Figure 11 – SNR analysis of the relative density variability.

The suspension prepared with the smallest particles combined with the highest solid loading and the highest rotation speed should lead to the highest homogeneity. Contrariwise, a combination of bigger particles, low solid loading and low rotation velocity would result in a more heterogeneous green cast.

The analysis of PSD for the suspension phase (0) and the green cast's cross-section (1– 5) can be seen in Figure 12. Here, $d_{p,k}^{*}$ is the previously defined normalized distance to mean diameter (Eq. 7). For all input parameters, the estimated values for the suspension region (0) vary in a wide range below zero. Since positive values indicate a higher proportion of bigger particles within a region and negative values a higher proportion of smaller ones, it can be reasoned that smaller particles are predominant in suspension after casting.

This behavior has been reported previously after the modeling, simulation and further experimental validation of similar systems (BIESHEUVEL et al., 2001; HONG, 1997b). It was observed that the PSD of particles in the suspension changes starting from the beginning of the rotation. The solid loading in the suspension decreases with casting time and so does the mean diameter of particles remained in suspension. Combining these results with information from Table 8, we can infer that this phenomenon is accentuated when the mean diameter is the lowest without statistically significant fluctuations due to other input parameters.
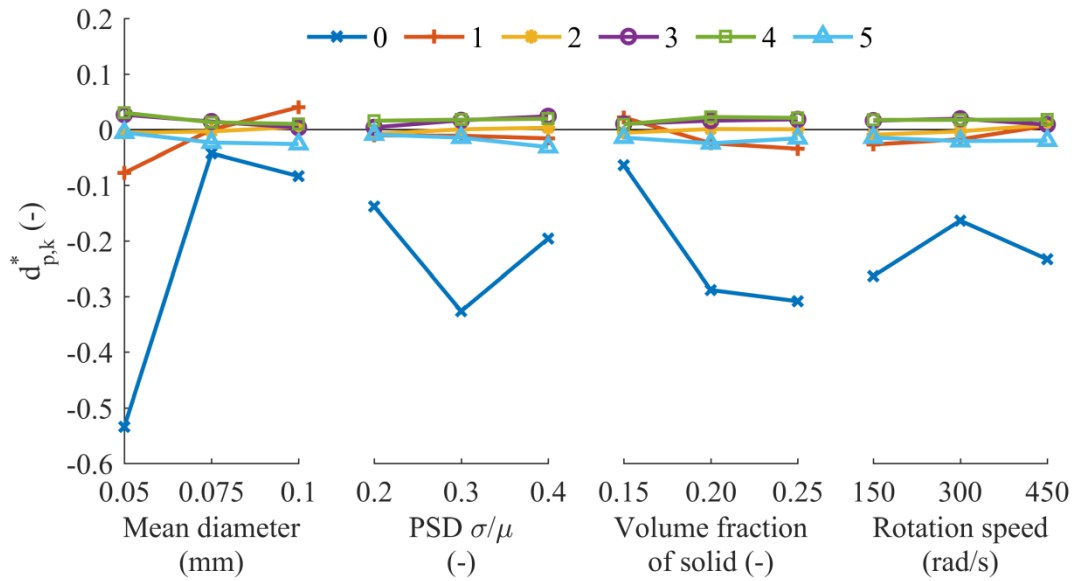
Figure 12 – Analyses of the normalized distance's average response from the starting powder's mean diameter for the suspension (0) and the green cast's cross-section from the inner (1) to outer (5) regions.

Another important aspect is that the PSD of the green cast along the cross-sections (1–5) does not seem to suffer as much variation as the suspension phase. Among the regions, the inner one (1) shows higher variation than the others. The mean diameter within this region is significantly affected by the mean particle size of the original powder. Here, the region's mean diameter seems to be lower than the original powder's mean when the lowest mean particle size is considered, indicating that the smallest particles prevail in the inner region. Contrariwise the behavior is the opposite for the highest mean diameter of the original powder.

Significant variations can be observed in the PSD through the SNR analysis (Figure 13) due to the particle mean diameter of the starting powder and its size distribution. Expecting size segregation when using small particles with a wide size distribution, green cast's normalized values oscillate within a range of [-0.1; 0.1], indicating that the distribution of particles is similar to the distribution of the original particle mixture.

For the system under study, the rotation speed –or angular velocity– is constant for all instants and radial positions, but particles will acquire different settling velocities depending on their diameter and distance from the center of rotation. For instance, considering a pair of particles, the smaller particle will gain a higher velocity than the bigger one only if they are at the same distance from the center. Due to the dependence on radial position, a particle located close to the center of the mold will gain an overall low velocity

while a particle in the vicinity of the wall with the same size will travel much faster towards it. As a consequence, particles located closer to the wall at the beginning of rotation will deposit on the mold faster as a whole, leaving no time for size segregation to occur, as it was observed across the green cast's cross-section, while the ones near the axis of the rotation will travel slower. Here, smaller particles can develop lower settling velocities than bigger particles, thus abandoning the suspension phase last.
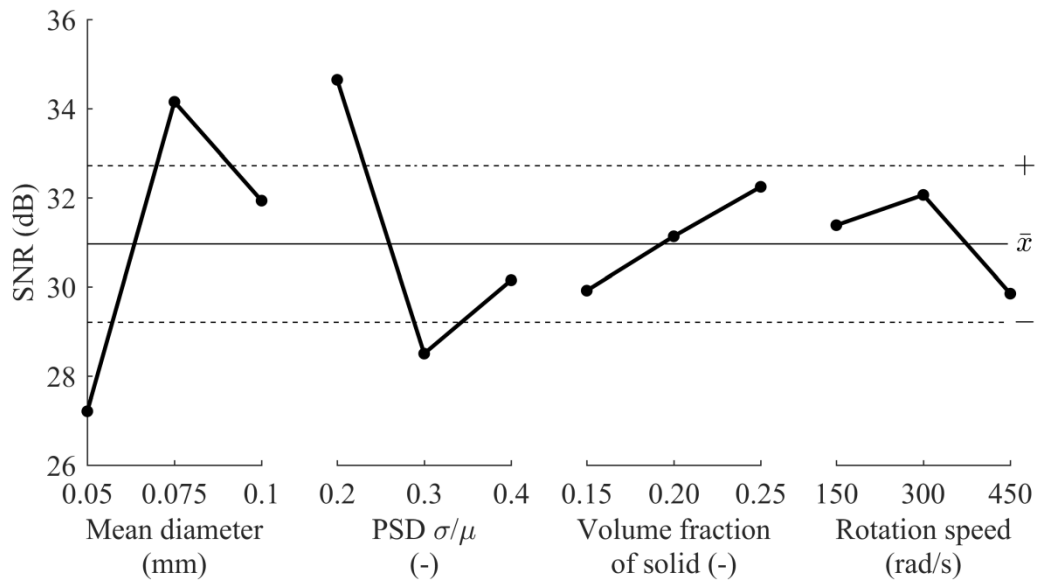
Figure 13 − SNR analysis of particle size distribution's variability along the cast's cross-section.

4.3 ASSESSMENT OF PARTICLE SEGREGATION ALONG THE CAST'S CROSS-SECTION

According to the results from SNR analysis for the particle size distribution over the cross-section (Figure 13), the starting powder's mean particle size and distribution influence the segregation by size significantly. The highest segregation is expected for the values that minimize the SNR, which are the smallest mean diameter, intermediate distribution, lowest solid loading and highest rotation speed. As a consequence, for further testing, there were chosen the mean particle diameter of 0.05 mm, a distribution of 0.3, a volume fraction of 0.15, and a rotation speed of 450 rad·s^{-1}. Since this combination of input parameters is not found in Table 4, it was added to the previously proposed *in silico* case studies, and the mixtures' characteristics for them are detailed in Table 9.

Table 9 – Overview of the case studies to analyze mixtures of powders.

Case study	Powder 1			Powder 2		
	Material	Mean diameter (mm)	Volume fraction[*] (-)	Material	Mean diameter (mm)	Volume fraction[*] (-)
C1	Alumina	0.05	0.9	Alumina	0.05	0.1
C2	Alumina	0.05	0.9	Nickel	0.05	0.1
C3	Alumina	0.05	0.9	Alumina	0.50[**]	0.1
C4	Alumina	0.05	0.9	Nickel	0.50[**]	0.1

[*]Dry basis [**]Mold radius modified to 12.5 mm

The volume fraction between powders was based on the literature (ZYGMUNTOWICZ et al., 2015). The results from these case studies are summarized in Table 10 and Figure 14, and links to simulation videos are given in Appendix A. The PSD of the suspension phase (0) and over the green cast's cross-section (1–5) had been evaluated by finding the mean particle diameter in every region. For case studies C2 and C4, performed with mixture of alumina and nickel, the volume fraction of nickel over the regions are also detailed.

Table 10 – Results from mixtures of powders.

Variable	Case study			
	C1	C2	C3	C4
Number of particles	28798	28798	4855494	4855494
Cast formation time (s)	0.021	0.023	0.026	0.024
Mean cast thickness (mm)	0.397	0.395	1.639	1.641
Relative density in 1 (−)	0.314	0.321	0.562	0.545
Relative density in 2 (−)	0.595	0.595	0.635	0.627
Relative density in 3 (−)	0.602	0.603	0.644	0.640
Relative density in 4 (−)	0.600	0.602	0.645	0.654
Relative density in 5 (−)	0.620	0.621	0.624	0.638

Due to the increased mold radius, the number of particles is much higher for case studies C3 and C4 (Table 10). The radius was increased for these studies because a group of particles was introduced into the suspension with a close diameter to the original mold (2.50 mm). This change led to an increase in cast thickness while casting time remained relatively similar, as predicted by Biesheuvel et al. (1998).
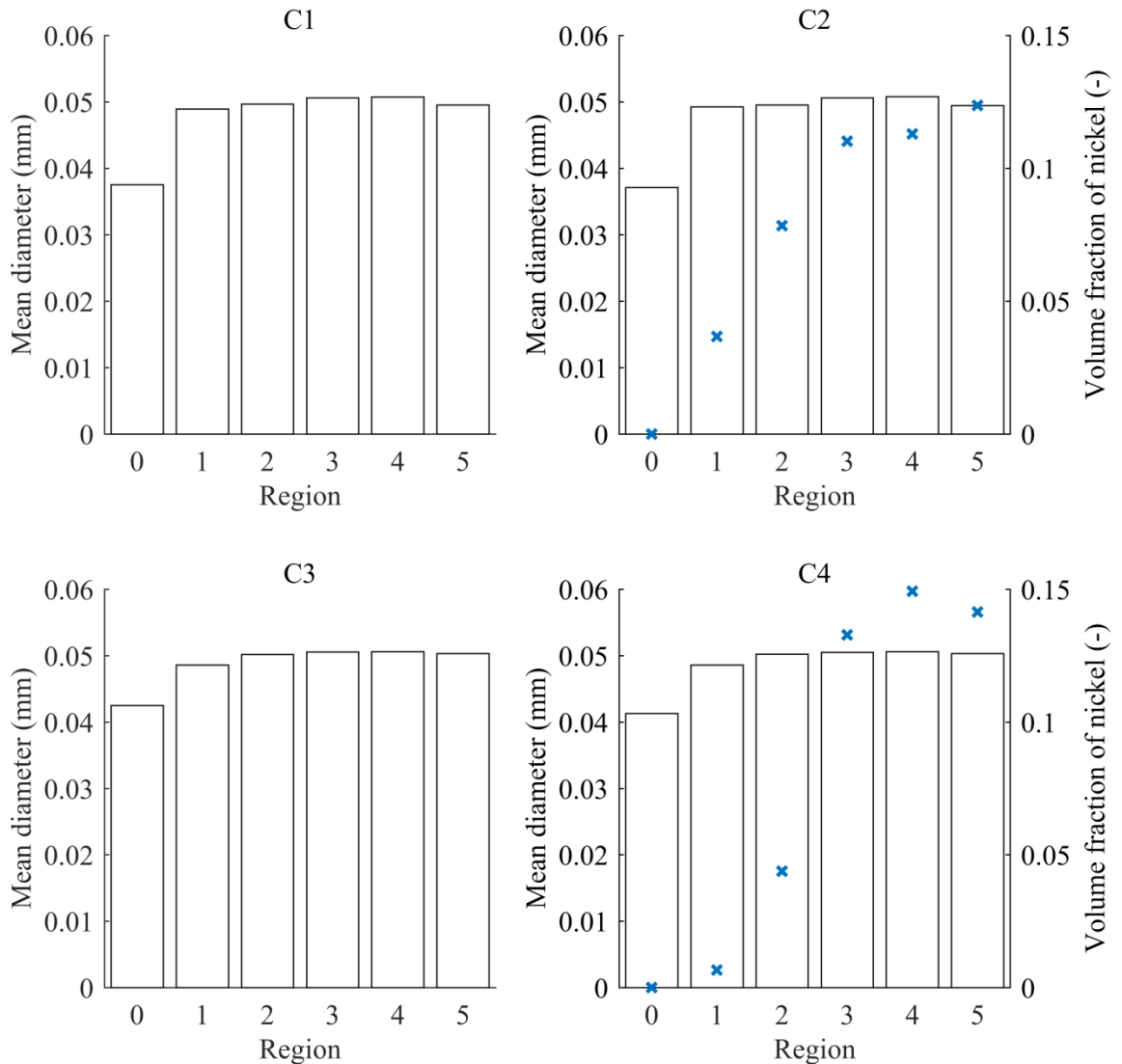
Figure 14 – Mean diameter (bars) and particle fraction of nickel (x-marks) per region for the suspension phase (0) and the cast's cross-section (1–5).

The determination of the relative density along the cast's regions shows a lower value for the inner (1) region again. The remaining four regions, which constitute 80% of the total thickness, exhibit similar values. As seen in the previous setups, they increase from the inner to the outer region for case studies C1 and C2. Here, there is no size variation between powders. However, the relative density seems to increase up to the center and decrease near the outer region for case studies C3 and C4 –where there is a significant size difference between powders. This behavior indicates a change in the cast's structure due to particle size variation.

The gradient of the mean particle diameter among regions for all the experiments can be seen in Figure 14. The results for case studies C1 and C2 follow similar trends. The mean diameters calculated for all regions among the cast are very close to the mean diameter of the starting powder, except for the suspension phase. Thus we can confirm that segregation by size is negligible when the size range is small, even using the configuration that should have led to the maximum segregation. Besides, when a fraction of a material with a different density is introduced into the suspension (case study C2), the formation of a graded structure can be observed, which is desired for several applications (SALEH et al., 2020). The fraction of denser particles increases gradually from the inner to the outer regions, as expected according to the basic principles of centrifugal casting.

Nevertheless, if two powders with a difference in the size of one order of magnitude are taken, the profile changes. Despite what was predicted by the literature (CARO, 2016; DE LA ROCHA et al., 2021), small particles do not necessarily stay at the inner region when bigger particles accumulate in the outer region even when they are of the same material. Case studies C3 and C4, with 90 vol.% of small particles and 10 vol.% of big ones, exhibit nearly the same particle size distribution results, very similar to the size distribution observed for C1 and C2. However, the volume fraction of nickel profile in C4 shows an increase on nickel content from region 1 (inner) to 4, but a decrease in region 5 (outer). Even though the inner layers follow the expected outcome, the drop in region 5 shows a bigger amount of smaller lighter alumina particles than expected in the outer layer. From these results, we can infer that small particles can move through the structure after entering the cast region, leaving the bigger particles behind when there is a considerable size difference among them, forming a segregated structure, hence a hierarchical one. The smaller particles' percolation also occurs for smaller particles with lower density than the bigger particles (case study C4)—this particle's percolation can also increase casting time.

Similar trends have been reported for powder mixtures used for centrifugal casting, where the bigger particles were also the denser ones (CHANG et al., 1991; SIVAKUMAR et al., 2003; ZYGMUNTOWICZ et al., 2015, 2018). For instance, an alumina-nickel aqueous suspension was rotated inside a mold by Zygmuntowicz et al. (2015, 2018) to assess the nickel profile along the cross-section considering a higher proportion of smaller and lighter particles as C4. After removing the remaining suspension, drying, and sintering, they observed three distinct regions:

- an inner region formed mainly by the smaller alumina particles;

- an intermediate region with increasing nickel content up to a maximum value;
- an outer region with decreasing nickel content.

The formation of the latter region can only be explained by smaller particles crossing the voids originated by particle packing, thus traveling up to the mold's surroundings since they do not find a barrier to stop them.

Finally, the almost-pure alumina layer formation can be explained by the alumina excess and by the remaining suspension withdrawal after centrifugation. When the liquid is poured out of the mold, a suspension layer coats the green tube's inner region due to the no-slip condition developed against it. After that, the inner surface remains wet, and the cast's pores are filled with suspension, and any trace of it leaves its solid content behind when the water is evaporated. The lighter fluid phase stays on the central region and its solid fraction is constituted mainly by smaller and lighter alumina particles, as previously mentioned.

4.4 EXPERIMENTAL

The experiments hereafter discussed are detailed in Table 11. Their main goal is to explore the effect of particle segregation by size and density using bench experiments that correspond to the setup shown in Table 9. For these experiments, powders containing particles with even smaller sizes than previously used in this work were chosen to favor segregation, but their size distribution was the one provided by the manufacturers. The same rotation speed as the *in silico* case studies was used for the rotation, and the solid loading was increased in order to obtain thicker casts since this variable's effect is negligible according to the SNR analysis (Figure 13).

Table 11 – Detail of experiments using powder mixtures.

| Experiments | Powder 1 | | Powder 2 | | Equivalent case study |
	Material	Volume fraction (-)	Material	Volume fraction (-)	
D1	Alumina	1	–	–	C1
D2	Alumina	0.9	YSZ	0.1	C2
D3	Alumina	0.9	Titania	0.1	C3
D4	Alumina	0.9	Nickel	0.1	C4

After shaping and drying, green tubes' samples were extracted and the SEM images of their inner and outer surfaces are shown in Table 12. The highest magnification achieved was 5000x and allows the observation of details in a micrometric scale, i.e., particles could be observed in the captured images, except for nanometric titania particles. At this scale, experiments D1 and D2, which correspond to mixtures of powders with similar mean sizes, do not show much difference between inner and outer surfaces' images.

Since the precursor powders are not monosized, the characteristics of the cross-section were also evaluated for experiment D1 performed with pure alumina (Figure 15). The lower magnification (100x) suggests a variation on the structure along the cross-section, but the magnified images captured on the vicinities of the inner and outer regions do not indicate significant difference regarding particle sizes.

Meanwhile, when using particles with similar sizes but different densities, the formation of a functionally graded structure was expected according to the equivalent *in silico* case studies. The EDS analyses' images for all experiments are shown in Table 13, and the results for experiment D2 using an alumina-YSZ mixture show very similar zirconium proportion against aluminum on the inner, outer and cross-section surfaces. However, these results cannot be interpreted as homogeneity along the cross-section since zirconium and gold peaks were overlapped leading to an inconclusive observation.

When particles with size differences of one order of magnitude are considered, as in experiments D3 and D4, it is expected to observe segregation according to the *in silico* case studies. Looking only at the SEM images in Table 12, not much difference can be observed contrasting the inner and the outer surfaces for experiment D3, where the smaller particles should have percolated through the cast, and segregation due to density differences should be negligible. Nevertheless, the highest magnification employed was not high enough to distinguish nanometric titania particles. The EDS images (Table 13) show a nearly homogeneous distribution of titanium along the cross-section; however, the mass fraction of titanium determination indicates that its content decreases from inner to outer regions.

Finally, the SEM images for experiment D4 show a difference between the inner and the outer surfaces. In this case, bigger particles appear on the latter surface. Experiment D4's EDS analysis results show that the nickel content in the inner surface is nearly zero, it grows up to a maximum value, and decreases near the outer region. These results agree with the trends reported by Zygmuntowicz et al. (2015, 2018) and with the case study C4 with particles of different sizes and densities.

Table 12 – SEM images.
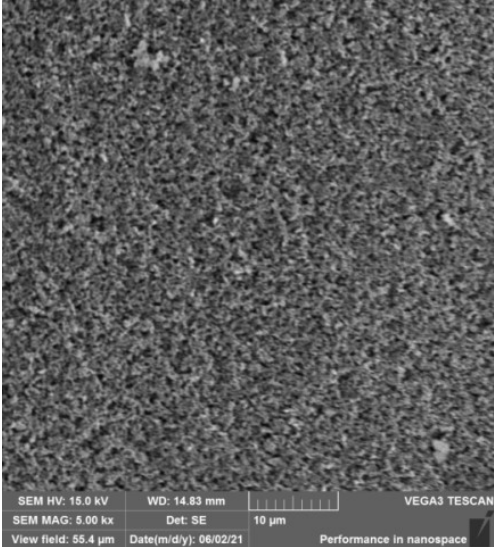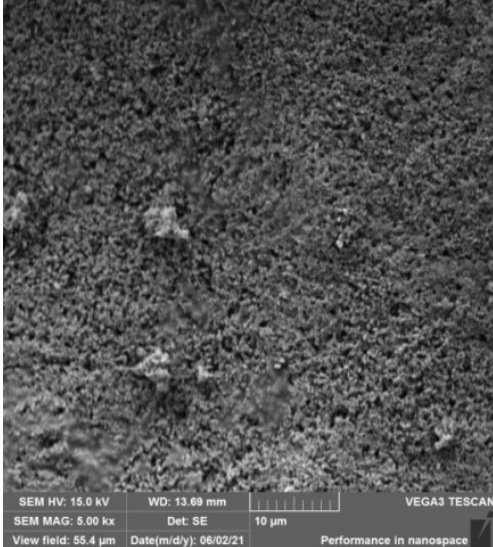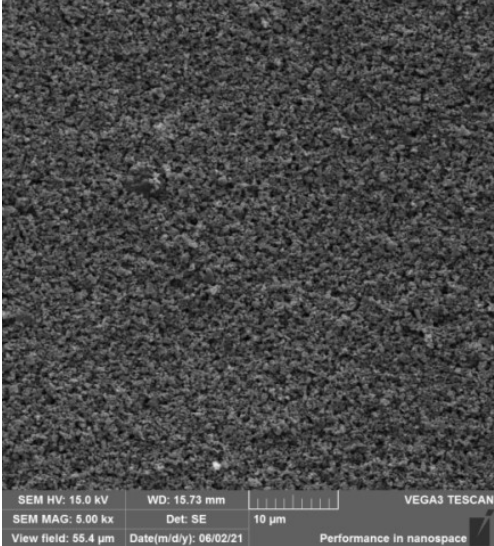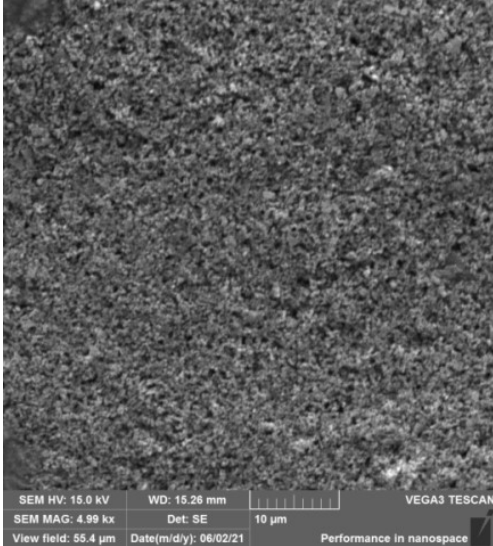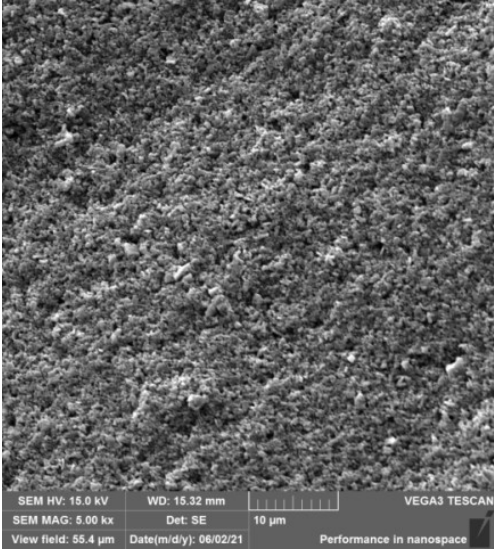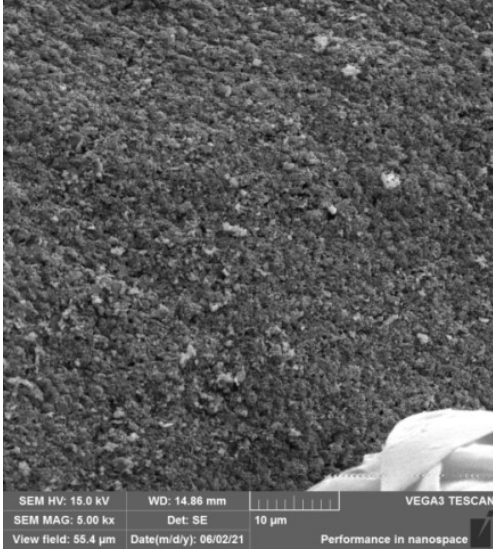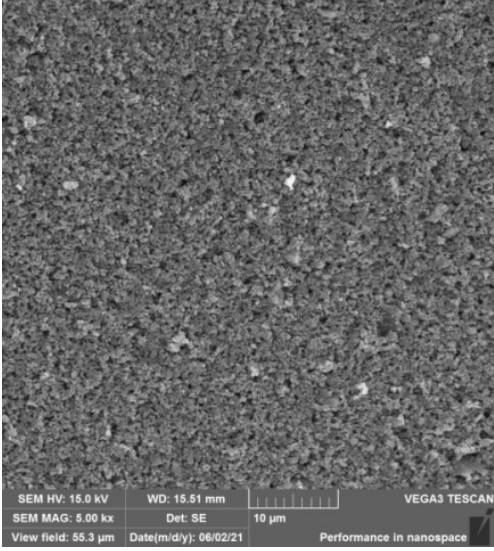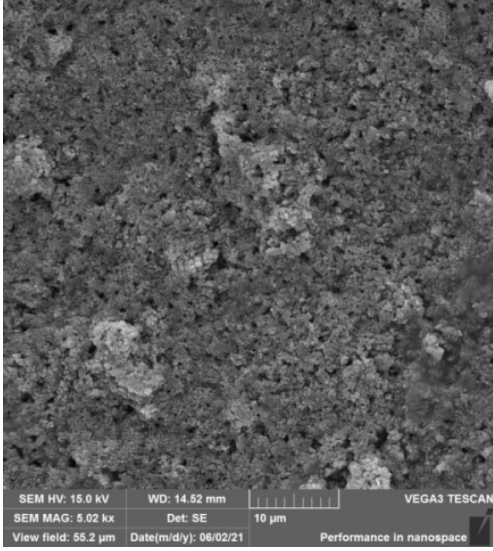
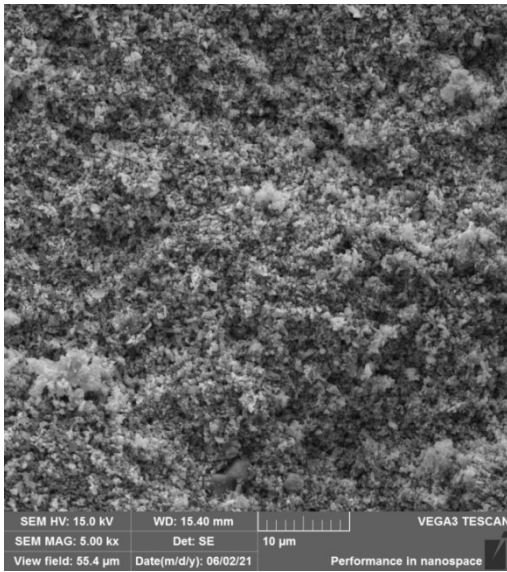| Experiment	Inner surface 5000x	Outer surface 5000x
D1		
D2		

Table 12 – SEM images (cont.).

Experiment	Inner surface 5000x	Outer surface 5000x
D3		
D4		

Cross-section (100x)
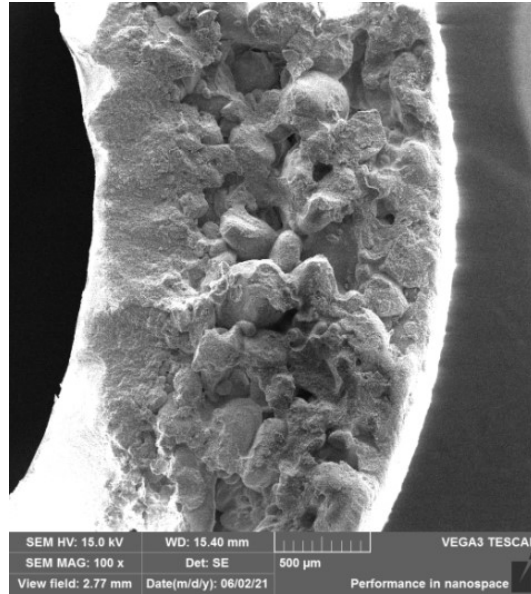
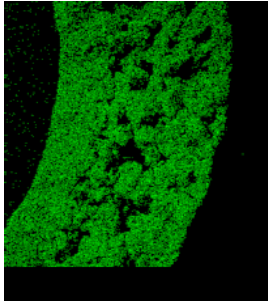Inner cross-section surface (5000x)   Outer cross-section surface (5000x)
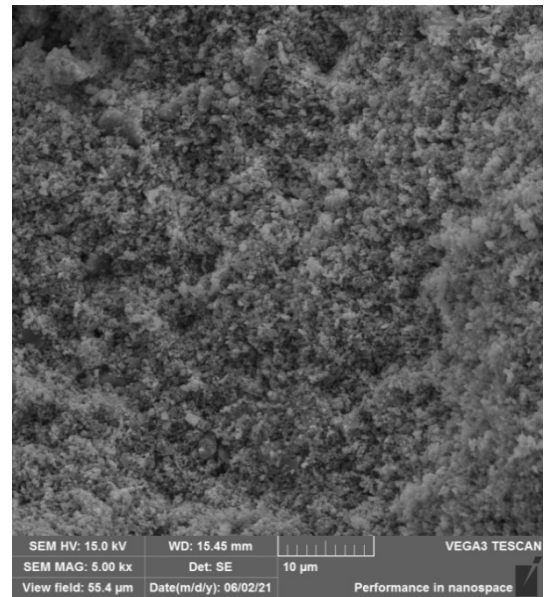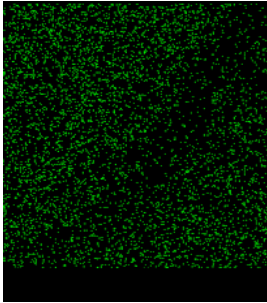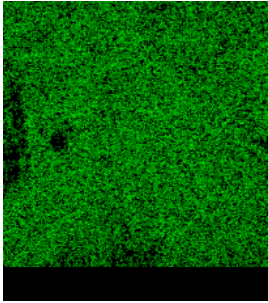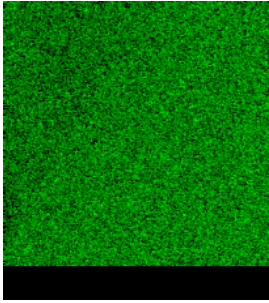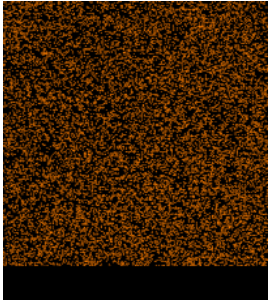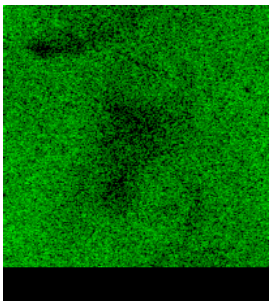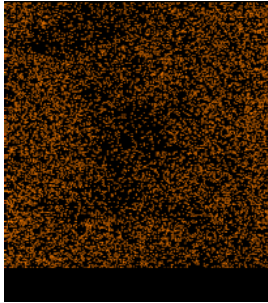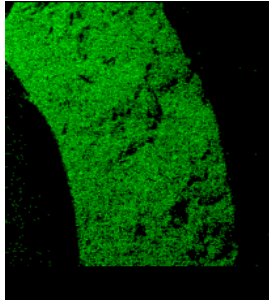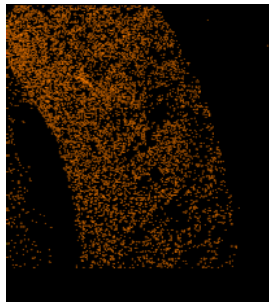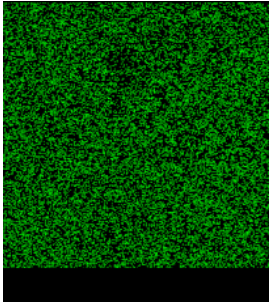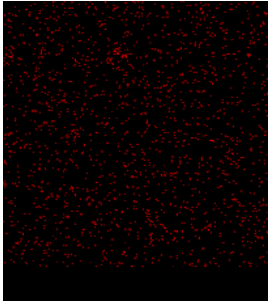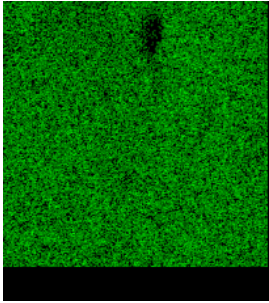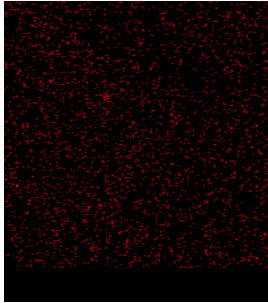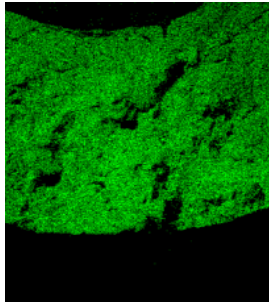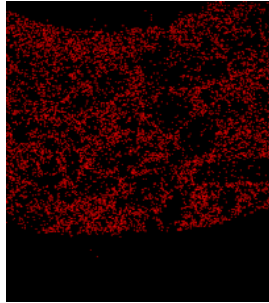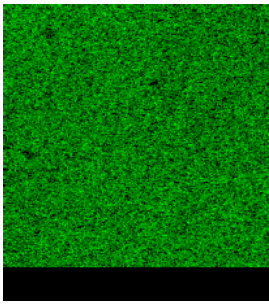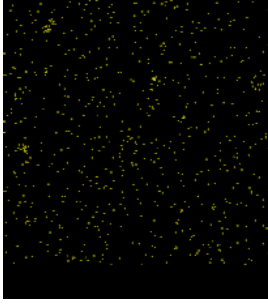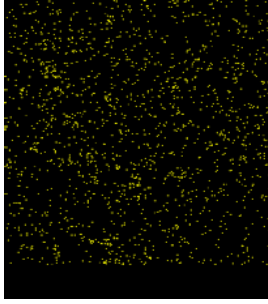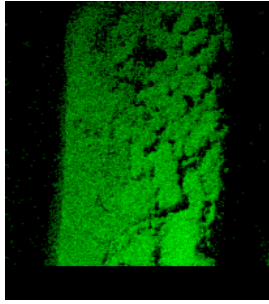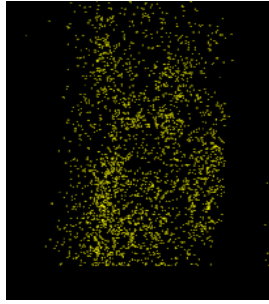
Figure 15 – SEM images of alumina (experiment D1) green tubes.

Table 13 – EDS analyses results.

Experiment	Inner surface		Outer surface		Cross-section	
D1						
	Al: 1		Al: 1		Al: 1	
D2						
	Al: 0.751	Zr: 0.249	Al: 0.769	Zr: 0.231	Al: 0.789	Zr: 0.211

Numerical values below images indicate mass fractions (–).

Table 13 – EDS analyses results (cont.).

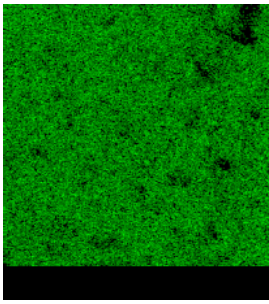| Experiment	Inner surface		Outer surface		Cross-section	
D3	Al: 0.834	Ti: 0.166	Al: 0.913	Ti: 0.087	Al: 0.859	Ti: 0.141
D4	Al: 1.000	Ni: 0.000	Al: 0.915	Ni: 0.085	Al: 0.852	Ni: 0.148

Numerical values below images indicate mass fractions (–).

5 FINAL REMARKS

After the comparison with results obtained from models of the literature, it can be concluded that the simulations performed using a DEM-based simulation can successfully reproduce *in silico* the centrifugal casting process with outstanding accuracy.

The cast thickness depends mainly on the solid loading, while the other tested parameters have a negligible effect on that variable. Small-sized particles with narrow distributions and high rotation velocities promote higher roundness. The solid load and rotation speed increase the cast relative density.

The particles located near the wall at the beginning of rotation are driven faster by stronger forces to the wall and are pressed against each other by layers and layers of solid, originating a more compact structure in the outer regions, resulting in a less dense inner layer and particle negligible segregation, except for significant size differences (one order of difference in this work).

Centrifugal casting is an ideal technique to obtain straightforwardly functionally graded materials for several applications such as ceramic membrane manufacture. The density differences can be exploited to obtain composition profiles, but depend more on the size difference among powders than on the density difference, therefore, both parameters must be fine-tuned to obtain the desired outcome.

REFERENCES

BELL, I. H. et al. Pure and Pseudo-pure Fluid Thermophysical Property Evaluation and the Open-Source Thermophysical Property Library CoolProp. **Industrial & Engineering Chemistry Research**, v. 53, n. 6, p. 2498–2508, 12 fev. 2014.

BERTOTTO, R. C. T. et al. Influence of sintering temperature on the development of alumina membrane shaped by centrifugal casting for gas separation. **Cerâmica**, v. 65, p. 99–103, jan. 2019.

BIESHEUVEL, P. M. et al. Graded membrane supports produced by centrifugal casting of a slightly polydisperse suspension. **Chemical Engineering Science**, v. 56, n. 11, p. 3517–3525, 1 jun. 2001.

BIESHEUVEL, P. M.; NIJMEIJER, A.; VERWEIJ, H. Theory of batchwise centrifugal casting. **AIChE Journal**, v. 44, n. 8, p. 1914–1922, 1998.

BISSETT, H.; ZAH, J.; KRIEG, H. M. Manufacture and optimization of tubular ceramic membrane supports. **Powder Technology**, v. 181, n. 1, p. 57–66, 30 jan. 2008.

CARDARELLI, F. **Materials Handbook: A concise desktop reference**. 3. ed. Switzerland: Springer, 2018.

CARO, J. Hierarchy in inorganic membranes. **Chemical Society Reviews**, v. 45, n. 12, p. 3468–3478, 13 jun. 2016.

CHANG, J. C. et al. Centrifugal Consolidation of Al2O3 and AI2O3/ZrO2 Composite Slurries vs Interparticle Potentials: Particle Packing and Mass Segregation. **Journal of the American Ceramic Society**, v. 74, n. 9, p. 2201–2204, 1991.

CUNDALL, P. A.; STRACK, O. D. L. A discrete numerical model for granular assemblies. **Géotechnique**, v. 29, n. 1, p. 47–65, 1 mar. 1979.

DE LA ROCHA, M. R. et al. Preparation of alumina based tubular asymmetric membranes incorporated with coal fly ash by centrifugal casting. **Ceramics International**, v. 47, n. 3, p. 4187–4196, 1 fev. 2021.

DOSTA, M.; ANTONYUK, S.; HEINRICH, S. Multiscale Simulation of Agglomerate Breakage in Fluidized Beds. **Industrial & Engineering Chemistry Research**, v. 52, n. 33, p. 11275–11281, 21 ago. 2013.

DOSTA, M.; SKORYCH, V. MUSEN: An open-source framework for GPU-accelerated DEM simulations. **SoftwareX**, v. 12, p. 100618, 1 jul. 2020.

DRIOLI, E.; GIORNO, L. (EDS.). **Encyclopedia of Membranes**. Berlin Heidelberg: Springer-Verlag, 2016.

FALAMAKI, C.; VEYSIZADEH, J. Taguchi design of experiments approach to the manufacture of one-step alumina microfilter/membrane supports by the centrifugal casting technique. **Ceramics International**, v. 34, n. 7, p. 1653–1659, 1 set. 2008.

GITIS, V.; ROTHENBERG, G. **Ceramic membranes: new opportunities and practical approaches**. 1. ed. Germany: Wiley-VCH Verlag GmbH & Co. KGaA, 2016.

GUAN, K. et al. Evolution of porosity, pore size and permeate flux of ceramic membranes during sintering process. **Journal of Membrane Science**, v. 520, p. 166–175, 15 dez. 2016.

HARABI, A.; BOUZERARA, F.; CONDOM, S. Preparation and characterization of tubular membrane supports using centrifugal casting. **Desalination and Water Treatment**, v. 6, n. 1–3, p. 222–226, 1 jun. 2009.

HERTZ, H. R. Über die Berührung fester elastischer Körper. **Journal für die reine und angewandte Mathematik**, v. 92, p. 156–171, 1882.

HONG, C.-W. Discrete Element Modeling of Colloidal Packing Dynamics during Centrifugal Casting. **Journal of the Ceramic Society of Japan**, v. 104, n. 1213, p. 793–795, 1996.

HONG, C.-W. New Concept for Simulating Particle Packing in Colloidal Forming Processes. **Journal of the American Ceramic Society**, v. 80, n. 10, p. 2517–2524, 1997a.

HONG, C.-W. Computer-Aided Process Design for Forming of Pore-Gradient Membranes. In: SHIOTA, I.; MIYAMOTO, Y. (Eds.). . **Functionally Graded Materials 1996**. Amsterdam: Elsevier Science B.V., 1997b. p. 29–34.

ISSAOUI, M.; LIMOUSY, L. Low-cost ceramic membranes: Synthesis, classifications, and applications. **Comptes Rendus Chimie**, Second international symposium Clays and ceramics for environmental applications. v. 22, n. 2, p. 175–187, 1 fev. 2019.

KIECKHEFEN, P. et al. Possibilities and Limits of Computational Fluid Dynamics–Discrete Element Method Simulations in Process Engineering: A Review of Recent Advancements and Future Trends. **Annual Review of Chemical and Biomolecular Engineering**, v. 11, n. 1, p. 397–422, 2020.

KIM, K.-H. et al. Centrifugal casting of alumina tube for membrane application. **Journal of Membrane Science**, v. 199, n. 1, p. 69–74, 30 abr. 2002.

LI, K. **Ceramic membranes for separation and reaction**. England: John Wiley & Sons, 2007.

NIJMEIJER, A. et al. The preparation of tubular membrane supports by centrifugal casting. **American Ceramic Society Bulletin**, v. 77, n. 4, p. 95–98, 1998.

NUNES, S. P. et al. Thinking the future of membranes: Perspectives for advanced and new membrane materials and manufacturing processes. **Journal of Membrane Science**, v. 598, p. 117761, 15 mar. 2020.

SALEH, B. et al. 30 Years of functionally graded materials: An overview of manufacturing methods, Applications and Future Challenges. **Composites Part B: Engineering**, v. 201, p. 108376, 15 nov. 2020.

SIVAKUMAR, R. et al. Processing of mullite–molybdenum graded hollow cylinders by centrifugal molding technique. **Journal of the European Ceramic Society**, v. 23, n. 5, p. 765–772, 1 abr. 2003.

STEENKAMP, G. C. et al. Centrifugal casting of ceramic membrane tubes and the coating with chitosan. **Separation and Purification Technology**, v. 25, n. 1, p. 407–413, 1 out. 2001.

TAGUCHI, G.; CHOWDHURY, S.; WU, Y. **Taguchi's quality engineering handbook**. United States: John Wiley & Sons, 2005.

TSUJI, Y.; TANAKA, T.; ISHIDA, T. Lagrangian numerical simulation of plug flow of cohesionless particles in a horizontal pipe. **Powder Technology**, v. 71, n. 3, p. 239–250, 1 set. 1992.

ZYGMUNTOWICZ, J. et al. Alumina matrix ceramic-nickel composites formed by centrifugal slip casting. **Processing and Application of Ceramics**, v. 9, p. 199–202, 1 dez. 2015.

ZYGMUNTOWICZ, J. et al. Combined centrifugal-slip casting method used for preparation the Al2O3-Ni functionally graded composites. **Composites Part B: Engineering**, v. 141, p. 158–163, 15 maio 2018.

APPENDIX A – VIDEOS

Table A.1 presents YouTube links to videos showing particle settling during centrifugal casting for the case studies detailed in Table 9.

Table A.1 – YouTube links to case studies videos.

Case study	View	Link
C1	Size distribution	https://youtu.be/2GpRnBOXOgo
C2	Size distribution	https://youtu.be/2ksHseNIWkw
C2	Materials distribution	https://youtu.be/mKmpVvKJ2y4
C3	Size distribution	https://youtu.be/DZUIQsTWR8k
C4	Size distribution	https://youtu.be/GX2dhqzaZSM
C4	Materials distribution	https://youtu.be/9-D5lH9XFX0